15 Dec 2000



FINAL REPORT
Office of Naval Research Grant No. N00014-96-1-0962

# CONSTRUCTION, CHARACTERIZATION, AND USE OF AN ARC-HEATED SUPERSONIC FREE-JET OF NITROGEN ATOMS FOR THE GROWTH OF GaN, AlN, AND InN THIN FILMS

R.B. Doak
Dept. of Physics and Astronomy
Arizona State University, Tempe, Arizona 85287-1504

# I. INTRODUCTION

This section summarizes briefly the research results and provides a chronology of how the research evolved. The students who contributed to this work are listed. It is interesting to note the initial experimental work with corona discharge free-jets was assigned to an undergraduate summer student, working in the laboratory as part of the ASU REU (Research Experience for Undergraduates) summer program under National Science Foundation funding. A list of the publications, talks, and patents resulting from this work is provided.

## Synopsis of Research and Results

Arc discharge and corona discharge supersonic free-jets are of interest as sources of "activated" nitrogen for molecular beam epitaxy (MBE) of nitride materials. Although the current objective is growth of III-V nitride semiconductors, these discharge sources are also very relevant to MBE of silicon-oxynitride gate dielectrics. Of interest in both applications is the relative ease and simplicity with which molecular species can be dissociated and/or electronically excited in electrical discharges. Very high temperatures may be attained in an arc discharge, allowing even the strong (9.76 eV) bond of the nitrogen molecule to be broken. If less power is required, as in non-dissociative electronic excitation, the lower power of the simpler corona discharge often suffices. By striking either type of discharge at the throat of a supersonic nozzle, a highly nonequilibrium distribution of dissociated and/or excited species from can be "frozen in" in the ensuing supersonic expansion, providing an intense beam of dissociated nitrogen atoms and/or excited nitrogen molecules. The exact spectrum of excited and/or dissociated species is determined by the type and power of the discharge. Both arc and corona discharge free-jet sources were constructed and tested in this work. The arc discharge supersonic free-jets (AD-SFJ) yielded beams consisting of up to 80% N atoms ($\sim 1 \times 10^{18}$ atoms $sr^{-1}$ $s^{-1}$) accompanied by undetermined amounts of excited atoms and molecules. The corona discharge supersonic free-jets (CD-SFJ) delivered metastable $A^3\Sigma_u^+$ $N_2$ molecules at up to 1.7% beam fraction ($9 \times 10^{16}$ metastables $sr^{-1}$ $s^{-1}$), accompanied by a small amount of $^4S^0$ ground state nitrogen atoms (less by a factor of ~10) and otherwise only non-reactive $X^1\Sigma_g^+$ ground state nitrogen molecules. Motivated by theoretical predictions that $A^3\Sigma_u^+$ should be an ideal species for MBE of III-N semiconductors, growth experiments were conducted with $A^3\Sigma_u^+$ of the CD-SFJ beam. The incorporation efficiency of $A^3\Sigma_u^+$ into GaN and AlN thin films was measured to be 50-100% under standard growth conditions, supporting predictions that $A^3\Sigma_u^+$ $N_2$ is a facile and easily incorporated reactant. The incorporation efficiency was independent of substrate temperature from 600 to 900 ° C, indicating direct dissociative chemisorption as the dominant reaction path. Optimum incorporation was obtained at a metal-to-$A^3\Sigma_u^+$ ratio of 1.5 while growing thin films of AlN, GaN, and AlN/GaN on 6H-SiC(0001) substrates at a rate of a few hundred Å per hour to thicknesses of 300-900 Å. Abrupt epitaxial interfaces were obtained under a variety of growth conditions with excellent overlayer crystallinity at temperatures of 700 ° C and above. The dominant growth morphology in the best of these relatively thin films was formation and coalescence of 2D islands having a height-to-width ratio of approximately unity in the final film.

## Chronological Retrospective

The basic thrust of this work was to improve MBE growth of III-N semiconductor thin films by developing novel molecular beam sources of reactive ("activated") nitrogen. Atomic nitrogen was the activation state that was initially of interest. An arc discharge supersonic free-jet (AD-SFJ) was built, tested, and shown to yield copious amounts of atomic nitrogen. Special graphite skimmers were developed to withstand the high temperature reactive SFJ plasma plume, which must be skimmed in order to produce the molecular beam. These graphite skimmers immediately became the skimmers of choice for gas discharge free-jet work. Before actual III-N growth experiments with the AD-SFJ could begin, theoretical work by Goddard and Muller [i] predicted that metastable molecular nitrogen rather than atomic nitrogen should be the preferred activation state. This conclusion was reached on the basis on reaction energetics, in particular on dissipation mechanisms for the large exothermicity of the activated nitrogen chemistry. Ground state ($^4S$) nitrogen atoms react readily, but the reaction is exothermic by 3.9 eV, all of which must be dissipated through the growing film. This is thought to lower the incorporation efficiency and may actually eject atoms from the film. These are major concerns, given that N vacancies may be responsible for the intrinsic high n-type doping of GaN. Ground state $N_2$ ($X^1\Sigma_g^+$) molecules do not react thermally with a GaN surface, 5.3 eV being required to dissociate and attach the two constituent atoms. Electronically excited $A^3\Sigma_u^+$ metastable $N_2$ molecules (6.2 eV above the ground state) do surmount this barrier. More importantly, Goddard and Muller predicted that as $A^3\Sigma_u^+$ reacts, one of its two atom carries away most (3.2 eV) of the heat of reaction, allowing the second to attach with only moderate (0.92 eV) excess enthalpy. Much less energy is therefore dissipated through the growing film. This was predicted to improve nitrogen incorporation and to minimize sputtering damage. To generate $A^3\Sigma_u^+$ molecules, the high power of an arc discharge is not needed. Instead a much simpler corona discharge supersonic free-jet (CD-SFJ) suffices. Moreover a CD-SFJ generates little or no excited atoms. This is an added advantage for GaN growth since, according to the Goddard and Muller's calculations, excited $^2D$ atoms abstract nitrogen from a GaN surface, thereby etching rather than depositing. Accordingly, our AD-SFJ research was redirected to CD-SFJ work. Relevant to this switch was also the fact that a second atomic nitrogen AD-SFJ effort was underway at the Jet Propulsion Laboratory [ii]. Although the rivalry was friendly and our laboratory enjoyed certain advantages, notably in beam diagnostic capabilities, the much higher funding level of the JPL effort made it clear that our expertise would be more fruitfully directed towards metastable molecular nitrogen beams. A CD-SFJ source was therefore built and fully characterized as to the type and flux of all reactive ("activated") nitrogen species in the beam. Growth experiments were carried out with this CD-SFJ, establishing the substrate temperature and metal-to-$A^3\Sigma_u^+$ ratio for optimum growth. The incorporation efficiency of $A^3\Sigma_u^+$ was measured in the course of this exploration, and found to indeed approach the predicted attachment of one nitrogen atom per incident $A^3\Sigma_u^+$ molecule.

---

[i] X.J. Chen, B. Tsai, S. Wang, and W.A. Goddard III, 2nd Workshop on Selected Energy Epitaxy (SEE-2), North Carolina State Univ., Raleigh, NC Jan 16-17, 1997.

[ii] F.J. Grunthaner, R. Bicknell-Tassius, P. Deelman, P.J. Grunthaner, C. Bryson, E. Snyder, J.L. Giuliani, J.P. Apruzese, and P. Kepple, J. Vac. Sci. Technol. A **16**, 1615 (1998).

## Student Participation

### Under direct ONR AASERT support:

Daniel G. Waters, Ph. D. Student, Arizona State University.

### Under support of parent ONR grant:

Victor M. Torres, Ph.D. Student, North Carolina State University.

### Under other support:

Christopher C. Burns, REU (Research Experience for Undergraduates) summer student, Arizona State University.

Dirk C. Jordan, Ph.D. Student, Arizona State University.

## Publications

### Overall Description of Research

(1) "A Corona Discharge Source for the Growth of III-V Nitrides," D.C. Jordan, Ph.D. Thesis, Arizona State University, December 1999.

(2) "Supersonic Beam Epitaxy of Wide Bandgap Semiconductors," V.M. Torres, D.C. Jordan, I.S.T. Tsong, and R.B. Doak, **Atomic and Molecular Beams - The State of the Art 2000, Part VII,** Chap 8, edited by R. Campargue, Springer-Verlag, Berlin, 2000, p. 945-958.

### Fabrication and Characterization of Refractory Graphite Skimmers

(3) "Refractory Graphite Skimmers for Supersonic Free-Jet, Supersonic Arc-Jet, and Plasma Discharge Applications," D.C. Jordan, R. Barling, and R.B. Doak, Rev. Sci. Instrum., 70, 1640-1648 (1999).

### Characterization of Corona Discharge Supersonic Free-Jet (CD-SFJ) Source

(4) "Corona Discharge Supersonic Free-Jet for III-V Nitride Growth via $A^3\Sigma_u^+$ Metastable Nitrogen Molecules," D.C. Jordan, C. Burns, R.B. Doak, J. Appl. Phys., **89**, 883-892, (2001).

### Measurement of $N_2$ $A^3\Sigma_u^+$ Incorporation Efficiency During GaN Growth

(5) "III-N Semiconductor Growth with Activated Nitrogen: A State-Specific Study of $A^3\Sigma_u^+$ Metastable $N_2$ Molecules," D.C. Jordan, I.S.T. Tsong, D.J. Smith, and R.B. Doak, Appl. Phys. Lett, 77, 3030-3032 (2000).

**Invited And Contributed Talks** (Name of presenter is underlined)

**Poster:** "Inexpensive Corona Discharge Source for the Growth of III-N Semiconductors," D.C. Jordan, C. Burns, and R.B. Doak, 15th Ann. Arizona Chap. Meeting of the Am. Vacuum Soc., May 11-14, 1998, Mesa, AZ.

**Invited Talk:** "Supersonic Free-Jet Epitaxy of Wide Bandgap Semiconductors," V.M. Torres, D.C. Jordan, I.S.T. Tsong, and R.B. Doak, 21st Int. Symp. on Rarefied Gas Dynamics, July 26-31, 1998, Marseille, France

**Seminar Talk:** "Supersonic Free-Jet Epitaxy of Wide Bandgap Semiconductors," V.M. Torres, D.C. Jordan, R.B. Doak, Seminar des Instituts für Grenzflächenforschung und Vakuumphysik, Forschungszentrum, Jülich, Aug 20, 1998 Jülich, Germany.

**Contributed Talk:** "Supersonic Corona Discharge Source for the Growth of III-N Semiconductors," D.C.Jordan, C.Burns, R.B.Doak, 45th International Symposium of the American Vacuum Society, Nov 2 - 6, 1998, Baltimore, MD.

**Seminar Talk:** "Supersonic Free-Jet Epitaxy of Wide Bandgap Semiconductors," V.M. Torres, D.C. Jordan, R.B. Doak, Seminar des Graduiertenkolleges, Ruhr-Universität Bochum, Oct 27, 1998, Bochum, Germany.

**Seminar Talk:** "Supersonic Free-Jet Epitaxy of Wide Bandgap Semiconductors," V.M. Torres, D.C. Jordan, R.B. Doak, Colloquium, Max-Planck-Institut für Strömungsforschung, Jan 22, 1999, Göttingen, Germany.

**Seminar Talk:** "Supersonic Free-Jet Epitaxy of Wide Bandgap Semiconductors," V.M. Torres, D.C. Jordan, and R.B. Doak, Universität Konstanz, Feb 5, 1999, Konstanz, Germany.

**Seminar Talk:** "Supersonic Free-Jet Epitaxy of Wide Bandgap Semiconductors," V.M. Torres, D.C. Jordan, and R.B. Doak, Commissariat à l'Energie Atomique, Département de Recherche sur l'Etat Condensé, les Atomes et les Molécules, Service de Recherche sur les Surfaces et l'Irradiation de la Matière, Saclay, France April 15, 1999.

**Seminar Talk:** "Supersonic Free-Jet Epitaxy of Wide Bandgap Semiconductors," R.B. Doak, Universität Regensburg, Regensburg, Germany, June 24, 1999.

**Contributed Talk:** "Corona Discharge Source for the Growth of III-V Nitrides," D.C. Jordan, B. Wilkens, I.S.T. Tsong, and R.B. Doak, Four Corners Meeting, Am. Phys. Soc., 1-2 Oct 1999, Tucson, AZ (awarded prize

for best student talk of session).

**Contributed Talk: Contributed Talk:** "Epitaxial III-V Nitride Growth on SiC(0001) by Means of $A^3\Sigma_u^+$ Metastable Molecular Nitrogen," D.C. Jordan, D.J. Smith, I.S.T. Tsong, and R.B. Doak, 47th Int. Symp. Am. Vacuum Soc., Boston, MA, Oct 2-6, 2000.

## Patent Activity

Provisional Patent Application # 60/092815, Filing Date July 14, 1998, "Refractory Graphite Skimmers for Supersonic Free-Jet, Supersonic Are-Jet, and Plasma Discharge Applications,"
D.C. Jordan, R.J. Barling, and R.B. Doak.

Provisional Patent Application # 60/213149, Filing Date June 22, 2000, "Novel Source of Activated Nitrogen and Method for Preparing Nitride Semiconductor Surfaces,"
R.B. Doak, C.T. Burns, and D.C. Jordan

## Format of Report

The presentation of scientific results, below, begins with a description of the fabrication and characterization of an arc-discharge supersonic free-jet AD-SFJ as a source of atomic nitrogen. The refractory graphite skimmers developed to skim this high temperature discharge are described in the second section. A discussion of the fabrication and characterization of a corona-discharge supersonic free-jet (CD-SFJ) makes up the third section. Growth experiments of GaN and AlN on 6H-SiC(0001) are presented in the fourth section, delineating the conditions for optimum growth and presenting measurements of the incorporation of metastable molecular nitrogen. The first section is an excerpt from the Ph.D. thesis listed as publication (1) in the above compilation of publications. The second, third, and fourth sections are publications (3), (4), and (5) from the list. Each section is introduced with a brief discussion of the work.

## II. ARC-DISCHARGE SUPERSONIC FREE-JET (AD-SFJ)

At the onset of this research, it was thought that atomic nitrogen would be the optimum activation state of nitrogen for the purposes of III-N semiconductor growth. Given the strong triple bond of the nitrogen molecule (9.76 eV binding energy), a temperature of several thousand degrees is needed to thermally dissociate molecular nitrogen to yield nitrogen atoms. Temperatures of this magnitude are available in arc discharges and arc discharge free-jets are reasonably amenable with standard molecular beam techniques. Accordingly, the fabrication and characterization of an arc discharge supersonic free-jet (AD-SFJ) was the initial goal of this research. The emphasis switched to a corona discharge free-jet (CD-SFJ) when theoretical work at Caltech indicated that the lowest triple metastable state of molecular nitrogen would actually be a preferred activation state over atomic nitrogen. For the sake of completeness and because a substantial amount of effort was invested in the arc discharge supersonic free-jet, this description of the arc-jet work is included, even though it was never published. This excerpt comes form the thesis of Dirk C. Jordan, "A Corona Discharge Source for the Growth of III-V Nitrides," Department of Physics and Astronomy, Arizona State University, December 1999.

## II. ARC-DISCHARGE SUPERSONIC FREE-JET (AD-SFJ) SOURCES

Dirk C. Jordan and R.B. Doak
Dept. of Physics and Astronomy
Arizona State University, Tempe, AZ 85284

An arc discharge is a high power electrical discharge characterized by high current (tens to hundreds of amperes) and low voltage ( a few to tens of volts) and an I-V curve of negative slope. A familiar arc discharge is the welding arc struck between a handheld anode and a metallic work piece. Confinement of the arc-welding discharge current to the small electrode surface yields extremely high current density and commensurately large joule heating, easily producing temperatures in excess of the melting point of most metals. This high current density is maintained by thermionic electron emission, a replenishing mechanism that sets the arc discharge apart from other discharges such as glow and corona discharges. The confined energy release of an arc discharge can also be used to good advantage in supersonic free-jet expansions to produce beams of otherwise unattainable species. The discharge is struck within the nozzle tube, heating the gas flow to produce electrically excited, and/or highly dissociated species just upstream of the nozzle throat. As the gas expands through the nozzle into vacuum, the gas density drops so abruptly that the gas is unable to fully thermalize, leaving high populations in excited/dissociated states. The core of this free-jet expansion can then be "skimmed" produce a beam of these species.

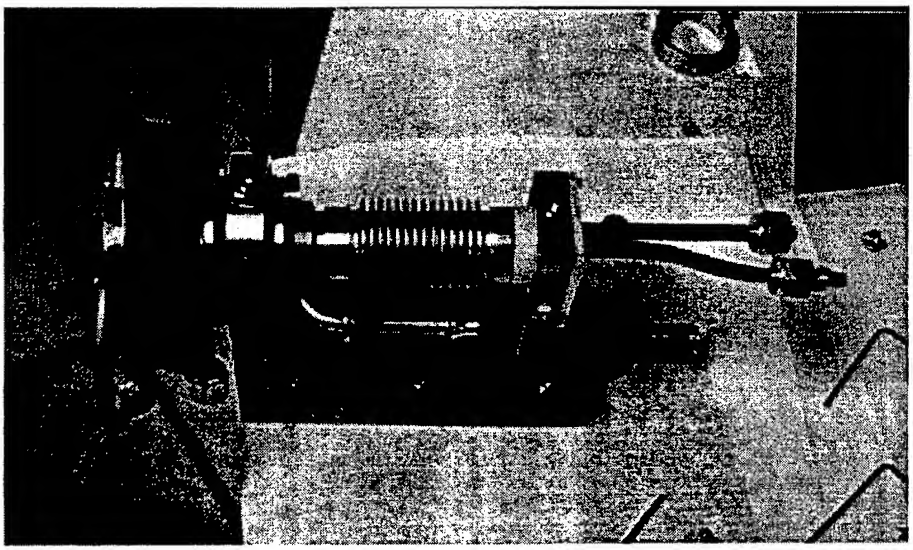

Fig. 1(a) Photo of AD-SFJ assembly, seen from the side. The nozzle, surrounded by a solenoid coil to produce a confining B-field, faces to the left in this image. A bellows assembly allows the anode-nozzle distance to be varied for striking and adjusting the discharge. The entire assemble is about 25 cm long.

In the arc-discharge supersonic free-jet source developed by Knuth and co-workers [1] and by Bickes, et al. [2], the discharge is struck between an anode within the nozzle tube and either the nozzle itself or a cathode positioned just downstream of the nozzle exit. With careful tailoring of the expansion flow through the nozzle, this discharge can be confined to the center of the gas flow through the nozzle tube, heating

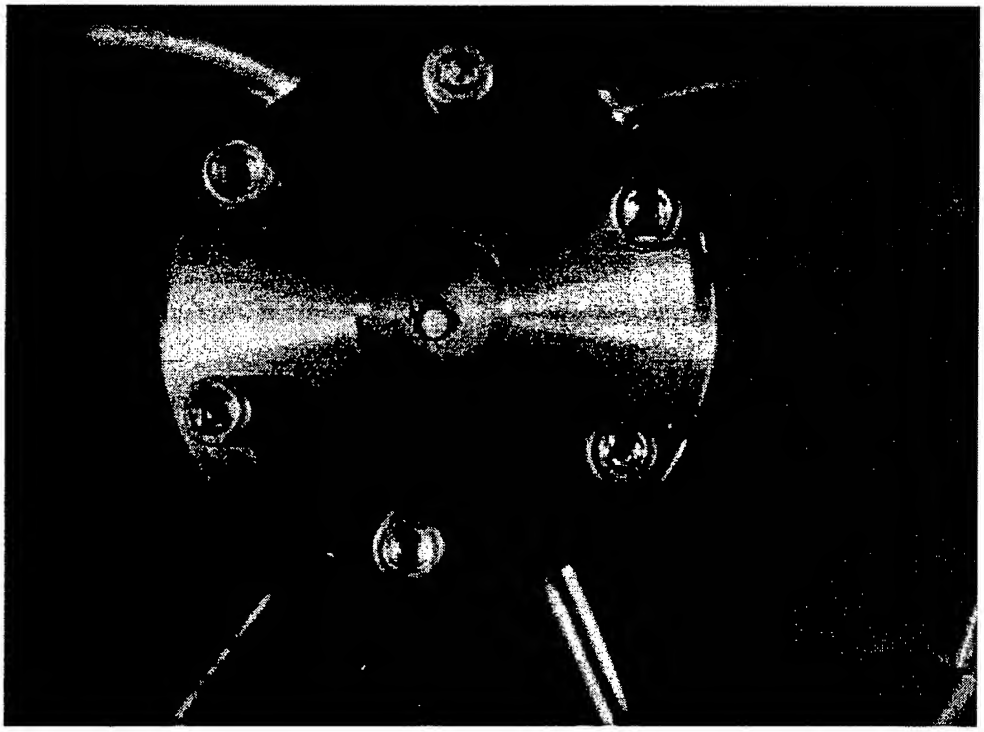

Fig. 1(b) Head-on view of a AD-SFJ nozzle aperture after about 50 hours of use. The solenoidal coil surrounding the water-cooled copper block has been dismounted in this image. A tungsten plate pressed into the copper block is drilled through to form the nozzle aperture. This plate also serves as the cathode for the discharge. The aperture has eroded to a significantly larger hole than its initial 1.25 mm diameter, allowing a clear view of the rounded cylindrical anode within the nozzle tube.

this region to temperatures of many thousand of degrees without destroying the nozzle tube or aperture. The very high local gas temperature suffices to break even the strong (9.76 eV) triple bond of molecular nitrogen, which is difficult to dissociate by other means.

Photos of the AD-SFJ nozzle are shown in Fig. 1(a) and 1 (b). The high power of the discharge (up to 1.5 kW) required that both the anode and the nozzle plate be water-cooled. For this purpose, the aperture plate was press-fitted into a water-cooled copper block as seen in Fig 1(b). A source gas was of premixed 8% nitrogen in argon was used in all of the AD-SFJ measurements. A 5 kW Sorensen power supply, Model DCR 32-155T, provided 0-32 VDC at 0-155 A to drive the discharge. The core of the supersonic free-jet was skimmed by special refractory graphite skimmers, developed explicitly for

this application as detailed later in this report. The resulting molecular beam was analyzed with an on-axis quadrupole mass spectrometer detector to determine its mass spectrum. Absolute measurements of the beam intensity were made using a "pitot" chamber.

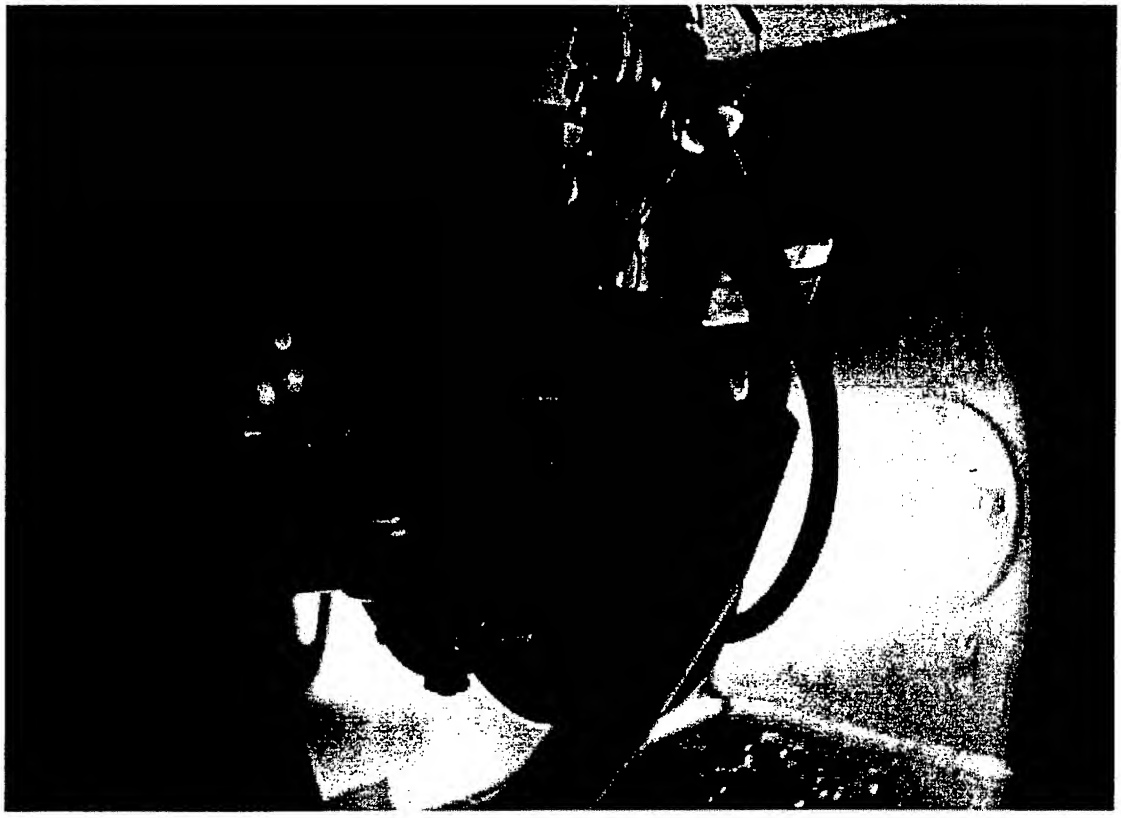

Fig. 2 The arc discharge supersonic free-jet (AD-SFJ) in operation in "external" arc mode, as photographed through the window of the vacuum chamber. The circular base of the refractory graphite skimmer is just visible to the right of the photo. The skimmer itself is obscured by the glare of the arc.

## Operation

The arc discharge would run in two very distinct working modes, denoted the "internal" and "external" modes. The internal arc was characterized by an intense white glow on the inside of the assembly and a low arc voltage, $U < 2$ V at a current of $I = 40$-$125$ A. The internal arc was readily obtained by "drawing" the arc, i.e. by bringing the cathode and anode in contact, applying the arc current then carefully separating the two electrodes. Since the plasma of the internal arc was confined to the inside of the nozzle tube, heavy electrode erosion often resulted. No atomic nitrogen could be detected in the terminal beam under internal arc conditions. Attempts were made to convert the internal arc to an external arc by increasing the stagnation pressure inside the

nozzle tube as describe by Bickes *et al.* [2]. These were invariably unsuccessfully, the internal arc simply extinguishing rather than converting.

The external arc was characterized by an intense blue-purple plasma plume downstream of the nozzle, as shown in Fig. 2. The power characteristics of the external mode, $U = 10 - 15$ V and $I = 60 - 100$ A, were significantly different from those of the internal arc. The external arc was established in two different ways, either by discharging a Tesla coil across the electrode gap, where the gap varied between 0.3 mm to 0.4 mm, or by very carefully bringing the electrodes into close proximity until the arc struck. The first method was the easier but could also result in an internal rather than an external arc. Although striking the external arc was non-trivial, once formed it could be maintained effortlessly for hours. The longest operation time was two hours and was limited by time constraints and not by arc instabilities. A self-wound electromagnet seemed to add to stability of the arc.

The external arc was operated at nozzle stagnation pressures of 650 torr and 900 torr, yielding a background pressure of ~100 mtorr in the source chamber pumped by a 17,000 l/s diffusion pump. The lower nozzle pressure led to more rapid electrode erosion than the higher. The 1.25 mm diameter tungsten nozzle aperture eroded quickly to larger diameters even with the external arc and could be used only a few times before replacement was necessary. Spark erosion cutting of nozzle apertures was prohibitively expensive at this rate of consumption, so alternative means of fabrication were developed. Diamond burs, usually used to polish gems, are available in various shapes and at low cost (<$15/piece). With careful cutting on a conventional milling machine, these tools were used to drill the necessary 1.25 mm apertures through the 1-2 mm thick tungsten nozzle plates. The graduate student working on this project developed these drilling techniques himself, after the ASU mechanical shops declared that such mechanical machining of tungsten was absolutely impossible.

**Characterization**

The fractional dissociation of nitrogen in the beam was established by measuring the partial pressures of atomic and molecular nitrogen. Values for these pressures were easily measured with the mass spectrometer detector, adjusting the raw counts on mass-to-charge ratios of 14 and 28 for the known ionization fragmentation yield of molecular nitrogen. Using Bickes' definition [72],

$$\alpha = \frac{0.5 P_N}{P_{N_2} + 0.5 P_N} \qquad (1)$$

where $P_N$ and $P_{N2}$ are the measured partial pressures for atomic and molecular nitrogen, respectively, the fractional dissociation was measured to be $\alpha = (84 \pm 9)\%$.

From the measured beam flux, the effective temperature of the gas within the nozzle discharge could be determined. The number flow rate of a supersonic expansion

is determined by the pressure $p_0$ and temperature $T$ within the source and by the effective nozzle diameter $d^*$,

$$\dot{N} = A\frac{p_0 d^{*2}}{\sqrt{T}} \quad , \tag{2}$$

where $A$ is a constant that can be calculated for any given gas mixture. Measurement of the argon flux in the 8% $N_2$ in Ar mixture gave T = (7590±910) K, which is somewhat lower than Bickes' results under similar conditions.

## References


[1] W.S. Young, W.E. Rodgers, and E.L. Knuth, Rev. Sci. Instrum., **62**, 2626 (1991)

[2] R.W. Bickes, Jr., K.R. Newton, J.M. Harrington, and R.B. Bernstein, J. Chem. Phys. **64**, 3648 (1976).

## III. EDM GRAPHITE SKIMMERS

To form a molecular beam, the isentropic core of a supersonic free-jet expansion must be collimated without disrupting the gas flow. This is not possible with a simple flat-plate aperture since back-scattering of the free-jet from the collimator plate severely disturbs the flow through the aperture. Rather, the aperture must take the form of a truncated cone, with the gas entering through a knife-edged orifice at the apex of the cone. Critical to this isentropic "skimming" of the beam is that the knife-edge of the conical "skimmer" be very sharp, the desired radius of curvature being 1 μm or less. Excellent skimmers of this quality are available commercially, fabricated via an electroplating process from nickel or copper, the only materials amenable to the electroplating. Although the nickel skimmers are amazingly robust to physical forces, their thin wall and relatively low melting temperature make them susceptible to melting and corrosion in an arc discharge. Although Tungsten and the natural ceramic "Lava" have therefore traditionally been used as skimmer materials for arc discharges beams, a sharp knife-edge cannot be formed on either of these materials. Following a suggestion from Ron Barling of the Mechanical Shop of the ASU Department of Physics and Astronomy, we fabricated skimmers from fine-grained graphite normally used in electrical discharge machining (EDM). In such machining, a die cut from the graphite is used to spark-cut the actual workpiece. Accordingly, the graphite is extremely refractory. We discovered that, with careful machining, a knife-edge cut onto an EDM graphite skimmer was limited only by the grain size of the graphite. Moreover, the machining could be done "free-standing," i.e. without a supporting mandrel. A very fined grain graphite (EDM-AF5, $< 1$ μm grain size) had recently been introduced by Poco Graphite and this allowed refractory graphite skimmers to be manufactured to nearly the same knife-edge sharpness as the state-of-the-art nickel skimmers. The following description of fabrication and testing of the EDM graphite skimmers was published as "Refractory Graphite Skimmers for Supersonic Free-Jet, Supersonic Arc-Jet, and Plasma Discharge Applications," D.C. Jordan, R. Barling, and R.B. Doak, Rev. Sci. Instrum., 70, 1640-1648 (1999).

# Refractory graphite skimmers for supersonic free-jet, supersonic arc-jet, and plasma discharge applications

D. C. Jordan, R. Barling, and R. B. Doak
*Department of Physics and Astronomy, Arizona State University, Tempe, Arizona 85287-1504*

(Received 16 July 1998; accepted for publication 10 December 1998 )

The fabrication of molecular beam "skimmers" from electrical discharge machining (EDM) graphite is reported. EDM graphite is highly refractory and is easily machined using conventional cutting and grinding techniques. In its most fine-grained form, EDM graphite can be machined free-standing to a knife-edge lip radius of $\sim 1$ $\mu$m, providing excellent skimmer aerodynamics. Being refractory, such EDM skimmers are of particular interest in sampling or collimating high-temperature plasma discharges. Our explicit application is in skimming an electrical discharge supersonic free-jet of molecular nitrogen, forming a molecular beam of $A\,^3\Sigma_u^+$ metastable $N_2$ to be used in the heteroepitaxial growth of III–N wide-band-gap semiconductors. In view of the their economy, ease of manufacture, and excellent aerodynamics, the skimmers may also find use in skimming conventional, nondischarge supersonic free-jets. The performance of the EDM skimmers was tested in a conventional helium supersonic free-jet expansion, measuring the time-of-flight distribution and beam intensity as a function of nozzle pressure and nozzle-skimmer separation. Direct comparison with commercial nickel and copper skimmers showed the EDM graphite skimmers to perform nearly as well as the best commercial metal skimmers. The refractory properties of the skimmers were tested in a high-temperature arc-discharge supersonic free-jet expansion of 10% nitrogen in argon. Exposure to a plasma plume of $\sim$7500 K for over 6 h produced only relatively minor deterioration of the EDM graphite skimmer. © *1999 American Institute of Physics.* [S0034-6748(99)04903-5]

## I. INTRODUCTION

Intense, highly monochromatic molecular beams can be formed by collimating the free-jet expansion from a supersonic nozzle.[1] The first stage of collimation takes place just downstream of the nozzle, in a region of very high beam density and flux. This precludes the use of a simple flat-plate collimator, which would generate a standing normal shock wave and stagnant boundary layer, seriously disrupting the flowfield at the collimator. An aerodynamic "beam skimmer" is therefore used. The skimmer is a hollow conical body truncated at its apex to form a knife-edged circular aperture. The skimmer base is mounted on the endwall of the nozzle chamber, the apex facing upstream into the free-jet. The axial core of the free-jet passes isentropically through the skimmer and out of the nozzle chamber, forming a well-defined beam. To yield an intense, nearly monoenergetic beam it is necessary that:[2,3]

(1) The skimmer must be longer than the stand-off distance of shock wave and boundary layer of the free-jet reflecting from the nozzle chamber endwall.

(2) The leading edge of the skimmer must be extremely sharp, allowing oblique conical shock attachment at the lip (if operating in a true hydrodynamic flow regime ) and avoiding backscattering from the lip (if in a more rarefied flow regime).

(3) The external apex angle of the skimmer must be sufficiently acute that the attached oblique shock does not detach to form a standing shock wave upstream of the skimmer. Yet the internal angle must not be so acute that the skimmed beam, still expanding, scatters from the internal wall of the skimmer.

Bossel and co-workers[2,3] tested long, slender skimmers (25°/32° full enclosed internal/external angle ) meeting these criteria and showed them to produce intense, near-isentropic beams. Such long, slender skimmers have become the accepted norm, finding applications in a wide variety of supersonic free-jet applications.[4]

The choice of skimmer material has no major impact on skimmer aerodynamics, provided the above criteria are fulfilled. The choice of materials is severely restricted by specifics of fabrication, however, particularly the critical step of forming the skimmer leading edge. Due to rounding and burring, it is not possible to cut a sharp free-standing knife edge on a ductile material. By electrodepositing material onto a conical mandrel, however, the knife edge can be cut with the supporting mandrel still in place.[5] A leading edge lip radius of $<1$ $\mu$m can be attained in this fashion. The electrodeposition process has therefore become the method of choice in skimmer manufacture, and virtually all high performance skimmers are consequently metallic. Nickel or copper skimmers are commercially available with 25°/30° full enclosed internal/external angles, having skimmer aperture diameters ranging from a fraction of one millimeter to several millimeters, and with a base-to-apex length of 1–3 cm.[6]

Metal skimmers are satisfactory for most supersonic beam applications but degrade rapidly if exposed to high temperatures, corrosive gases, or very energetic gas species.

0034-6748/99/70(3)/1640/9/$15.00

TABLE I. Characteristics of EDM graphite skimmer material.

| Property | Poco EDM-3 | Poco EDM-AF5 |
|---|---|---|
| Average particle size ($\mu$m) | <5 | <1 |
| Flexural strength (psi) | 13 500 | 17 000 |
| Compressive strength (psi) | 21 500 | 27 000 |
| Hardness (shore) | 76 | 87 |
| Electrical restivity ($\mu\Omega$ in.) | 540 | 680 |
| Apparent density (g/cm$^3$) | 1.81 | 1.80 |

This precludes the use of metal skimmers in most plasma discharge applications, particularly in arc-discharge supersonic free-jets.[7,8,9,10] Corrosion and overheating can be addressed by cooling the skimmer and by using refractory skimmer materials such as tungsten [11] or ceramic materials.[12] These tend to be expensive and imperfect solutions, however, representing a definite compromise among cost, ease of machinability, attainable sharpness of lip radius, and high-temperature durability. Inexpensive refractory skimmers with good aerodynamic characteristics would be of benefit to many skimmed beams applications including arc,[13,14] glow,[15] and corona[16] discharge supersonic free-jets as well as plasma discharge mass spectrometry.[17] In addition, there is currently extensive technological use of unskimmed discharges for materials growth[18] and processing,[19] much of which would likely benefit from beam skimming if suitably refractory skimmers were available. In a careful search of the literature we were able to find only a single reference to the use of graphite skimmers, namely, that of Valentini *et al.*[20] in crossed-beam experiments of halogen atoms and molecules. However, details of the quality, fabrication and use of those skimmers was never published.[21]

## II. EDM GRAPHITE SKIMMERS

We report the fabrication and testing of low cost refractory skimmers, machined free-standing from commercially available electrical discharge machining (EDM) graphite. Our first set of EDM skimmers was fabricated from Poco, Inc.[22] grade EDM-3 graphite having an average particle size of <5 $\mu$m. More recently we have fabricated skimmers from Poco grade EDM-AF5 graphite which has a still smaller average particle size of <1 $\mu$m. The properties of these graphites are listed in Table I. The material properties which make graphite so suitable for EDM applications also make the material an exceptional candidate for refractory skimmer applications. Electrical discharge machining is carried out by placing an electrode in near proximity to a workpiece, immersed in an insulating fluid, and pulsing a high voltage between the two pieces.[23] This gives rise to a spark discharge, producing extreme localized heating at the point of spark attachment, and removing material from the workpiece. As an EDM electrode material, graphite is economical, easy to machine, and quite refractory (an EDM "wear ratio" of 2.5, defined as the linear electrode consumption rate to workpiece removal rate). Moreover, graphite has good electrical conductivity, high thermal conductivity, high thermal shock resistance, high-temperature strength, and is available in forms having a very fine grain size. These are all desirable properties for refractory skimmer fabrication. Of particular importance is the small grain size, allowing a much sharper knife edge to be cut onto a graphite skimmer than can be achieved with other refractory materials such as the aluminum/magnesium silicate "Lava" [12] which has been used in many arc-jet applications.[8] For skimmer applications, it is the erosion of graphite under arc discharge in vacuum which is relevant. This has been measured [24] and found to be strongly dependent on the grain size, pore size, and electrical resistivity of the specific graphite variety. Measured erosion rates (mass removed per total electric charge exposure during the arc) ranged from $10^{-4}$ to $10^{-5}$ g/C.

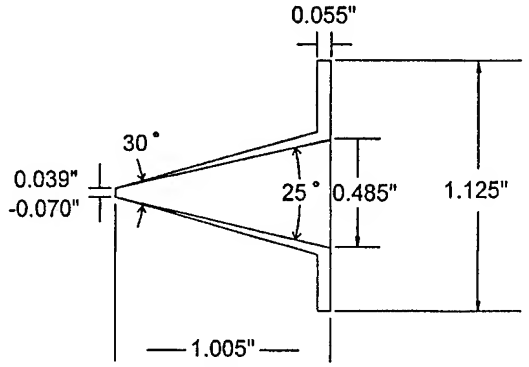


FIG. 1. Cross-sectional drawing of the fabricated EDM graphite skimmers.

## III. MACHINING

A cross section of the fabricated graphite skimmers is shown in Fig. 1. Machining is carried out on a standard lathe apart from a finishing cut on the outer skimmer sidewall, which is made on a horizontal grinder. The graphite rod stock is placed in the lathe chuck and the rod end faced off to form the sides and bottom of the annular skimmer base. The internal conical hollow of the skimmer is then cut into this base at full angle of 25°: An initial gross removal of material is made by stepped drilling, followed by a rough cut and then a fine cut of the interior skimmer wall, using appropriate cutting tools fabricated from standard lathe tool stock. Careful alignment of the cuts is critical to ensure that the axis of the interior conical hollow is aligned with the axis of the annular base. Long slender cutting tools and careful technique allow the interior apex of the cone on one sidewall to be cut without damaging the opposite sidewall. With the interior cavity completed and without altering the position of the rod stock in the lathe, the exterior wall of the skimmer is then rough cut to a full angle of 30°, eventually leaving the skimmer attached at its apex to the rod stock by a pedestal about 3 mm in diameter. A conical cut into this pedestal frees the workpiece from the rod stock. The skimmer is then moved to grinding machine to finish the exterior sidewall. The skimmer base, clamped into a custom jig, is mounted in the grinding machine such that the skimmer apex faces outwards. Careful alignment of the skimmer axis relative to that of the grinding machine is crucial to ensure that the final sidewall thickness is uniform and that the skimmer aperture is circular. A standard 7.5 in., 3600 rpm, 100 grit grinding wheel is used to grind the sidewall including, with particular

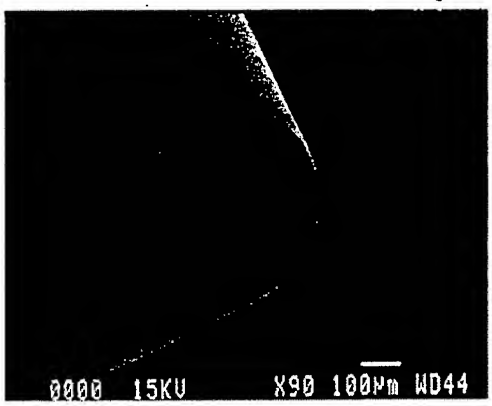


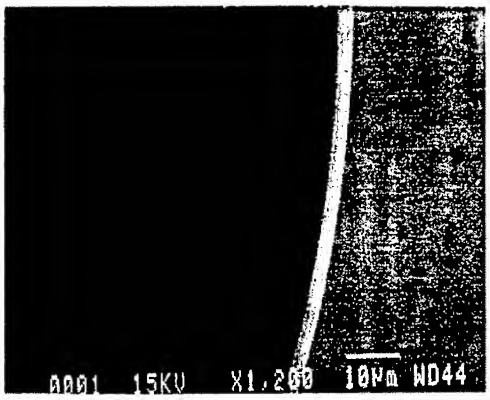


FIG. 2. SEM images of commercial nickel skimmer (see Ref. 6) at low (top) and high (bottom) magnification. Lengths scales of 100 $\mu$m (top) and 10 $\mu$m (bottom) are indicated by the horizontal bars.

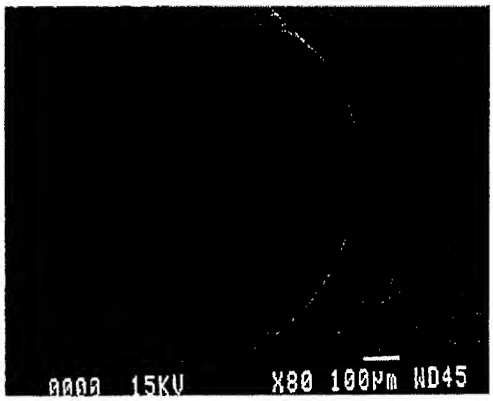


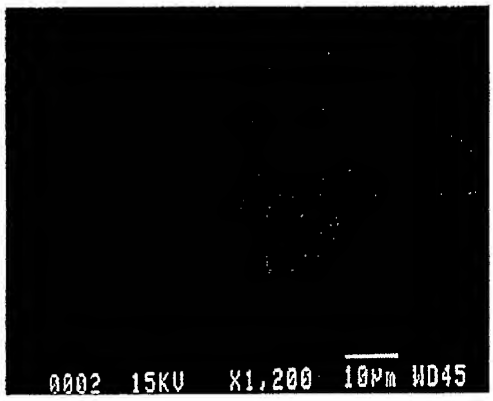


FIG. 3. SEM images of commercial rhodium-plated copper skimmer (see Ref. 6).

care, the remnants of the pedestal at the apex. This latter operation exposes and defines the skimmer aperture and the side wall is then ground back until the desired aperture diameter is achieved. This final grinding is viewed under a $\times 10$ binocular microscope. Total machining time for one skimmer is about four hours, not counting the initial fabrication of cutting tools and jigs.

## IV. SEM IMAGES OF SKIMMERS

Scanning electron microscopy (SEM) images of a commercial nickel skimmer,[6] fabricated by electrodeposition, are presented in Fig. 2. This skimmer is nearly flawless: the aperture is perfectly circular, the knife edge is uniform in thickness and profile, and the surface finish is smooth inside and out on a submicron length scale. In the higher magnification image the lip radius is seen to be 1 $\mu$m or less. This variety of skimmer clearly sets the standard for molecular beam skimmers. A rhodium-plated copper skimmer from the same company does not achieve the same high quality. As seen in the SEM images of Fig. 3, the orifice edge is much less regular in thickness, shows inconsistencies in the plating, has dendritic burrs attached to the periphery at several points, and is larger in lip radius by a factor of three or more.

SEM images of a typical graphite skimmer fabricated from EDM-AF5 are given in Fig. 4. This skimmer was machined free-standing as described above. The edge sharpness and surface finish are clearly limited by the particle size, quoted to be $<1$ $\mu$m for this material. However, the aperture edge is circular and well formed. The lip radius is seen to be about 1 $\mu$m—not appreciably worse than that of the commercial nickel skimmer. The knife edge displays a much grainier leading edge, however, due to the particulate nature of the EDM graphite.

SEM images of a typical EDM-3 graphite skimmer are presented in Fig. 5. As expected with the larger grain size ($<5$ $\mu$m) this knife edge shows an even more pronounced particulate structure and has a larger lip radius than the EDM-AF5 graphite skimmer. Within the limitation of grain size, however, the aperture is again quite circular and well defined. The lip radius, about 3 $\mu$m, is comparable to that of the commercial rhodium-plated copper skimmer although significantly more ragged in edge profile. Of interest is the interior finish on this skimmer, which appears to be *smoother* than that of the EDM-AF5 skimmer of Fig. 4 rather than worse. This may indicate that the grain size need not be an intrinsic limitation on the surface finish of the wall and that optimum machining techniques for the graphite have not yet been fully established.

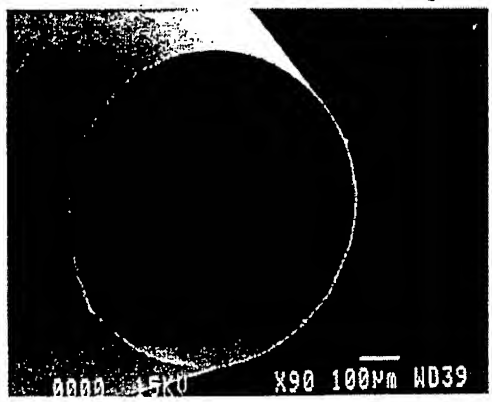


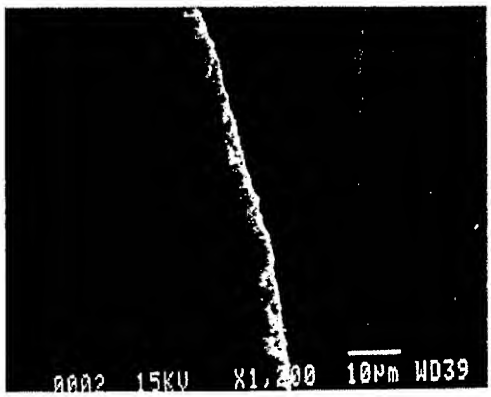


FIG. 4. SEM images of skimmer fabricated from Poco, Inc. EDM-AF5 graphite (1 $\mu$m average particle size).

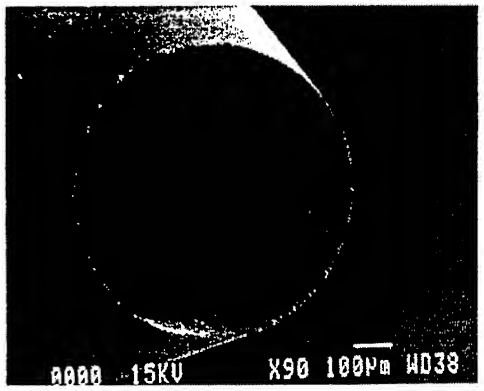


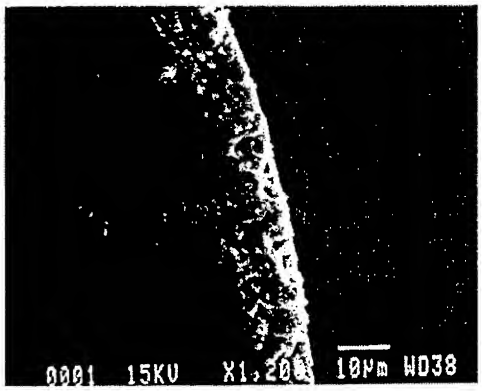


FIG. 5. SEM images of skimmer fabricated from Poco, Inc. EDM-3 graphite (5 $\mu$m average particle size).

An EDM-3 skimmer, similar to that of Fig. 5 but with orifice diameter of 1.6 mm, was tested for its refractory properties by exposing it to the plasma expansion of an arc-heated jet source of the Knuth type[7] running a mixture of 10% nitrogen in argon at an input power of 0.5–1.2 kW. The temperature of the plasma at the nozzle was estimated from source throughput measurements to be about 7500 K. The skimmer was exposed to this intense supersonic plasma plume for a total of 6 h with the skimmer apex situated 3.5 cm downstream of the nozzle. Figure 6 shows the SEM image of the skimmer apex following this treatment. The orifice edge has eroded discernibly and become planar, fully exposing the particulate structure of the graphite. The width of this planar lip edge is about 20 $\mu$m. As judged from the SEM length scale, the skimmer aperture does not appear to have increased significantly over its initial 1.6 mm diameter. The extremity of conditions to which the skimmer was exposed to can be judged from the solidified tungsten droplets (originating in sparking at the tungsten nozzle) observable on the inner skimmer edge. Yet even this bombardment with molten tungsten has not damaged the graphite wall.

## V. TIME-OF-FLIGHT MEASUREMENTS

Aerodynamic performance of the graphite skimmers was assessed with time-of-flight (TOF) measurements[4] of the beam velocity distribution. Both the apparatus and the TOF technique are described in detail elsewhere.[25] A supersonic free-jet expansion of helium from a 20-$\mu$m-diam nozzle was employed in this characterization. Measurements were made with the nozzle at both room temperature and at liquid-nitrogen temperature. Direct comparisons were made of a pristine EDM-3 graphite skimmer of 0.75 mm diam, a pristine EDM-AF5 graphite skimmer of 0.80 mm diam, and a commercial nickel skimmer of 0.50 mm diam. Each was used in turn to extract the core of the helium supersonic free-jet expansion and the velocity distribution of the resulting beam was measured via TOF. The chopper-detector distance was 3.76 m and the target-detector distance was 3.18 m. The channel width of the multichannel analyzer (MCA) was set to 2 $\mu$s. The chopper disk (two opposing 0.020 in. wide slits on a 4 in. diam) was run at a slit frequency of 500 Hz. Prior to each TOF measurement the source-skimmer distance was adjusted to maximize the beam intensity (see below).

The TOF measurements for a room temperature nozzle are presented in Fig. 7. The data in portions (a), (b), and (c) of that figure correspond to source stagnation pressures of

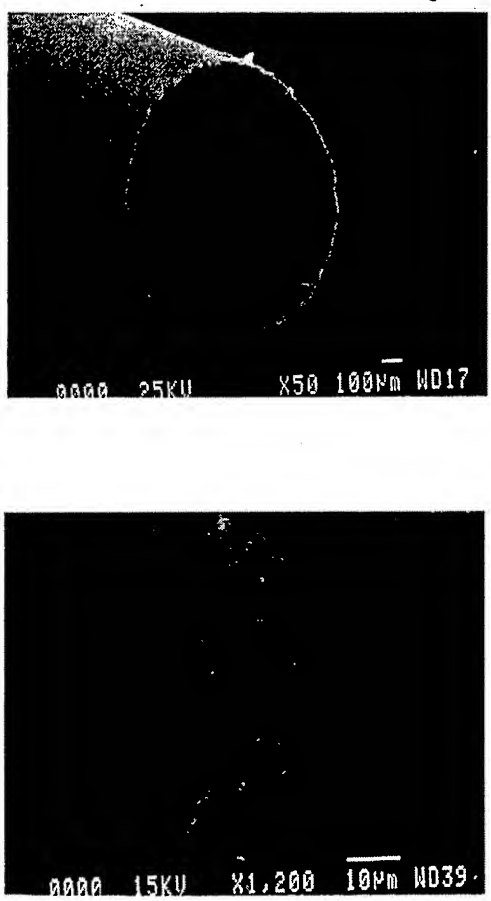


FIG. 6. SEM images of EDM-3 graphite skimmer after exposure to plasma plume of arc-discharge supersonic free-jet. Beads are solidified drops of tungsten.

50, 100, and 150 bar, respectively. To avoid overlap, the TOF curves for the EDM-AF5 and EDM-3 skimmers have been respectively offset along the time axis by +0.1 and +0.2 ms with respect to the TOF curve for the nickel skimmer. Given the long 3.76 m TOF path, velocity dispersion dominates the overall TOF width (i.e., exceeds the contributions from chopper shutter function and finite detector length). Thus the TOF peak widths of Fig. 7 provide a direct indication of the velocity distributions. To allow direct comparison of intensity among the various curves, the data have been scaled to a common emission current of 0.040 mA and a common total number of MCA sweeps of 50 000. A corresponding set of TOF curves with the nozzle at liquid-nitrogen temperature are shown in Fig. 8. The data in parts (a) and (b) of that figure correspond to stagnation pressures of 50 and 100 bar, respectively. TOF peak widths were extracted from Gaussian fits to the TOF curves. The TOF data are summarized in Table II.

From Fig. 7 and Table II it is seen that, for the room temperature nozzle, the graphite skimmers are quite competitive with the bellwether nickel skimmers. The TOF widths of beams produced by all three skimmers are essentially identical for the 50 and 100 bar source-pressures. At 150 bar small differences emerge, the $\Delta t/t$ increasing from 0.80% to 0.85% to 0.91% in progressing from Ni skimmer to EDM-AF5 skimmer to EDM-3 skimmer. This correlates with the increasing lip radius ($<1$ to $\sim 1$ to $\sim 3$ $\mu$m) and increasing graininess of the knife edge as seen in the SEM micrographs. Somewhat more pronounced are differences in TOF peak intensity. Relative to the TOF peak of the Ni skimmer, the TOF peak for the EDM-AF5 skimmer drops from 90% to 75% to 65% as the pressure is raised from 50 to 100 to 150

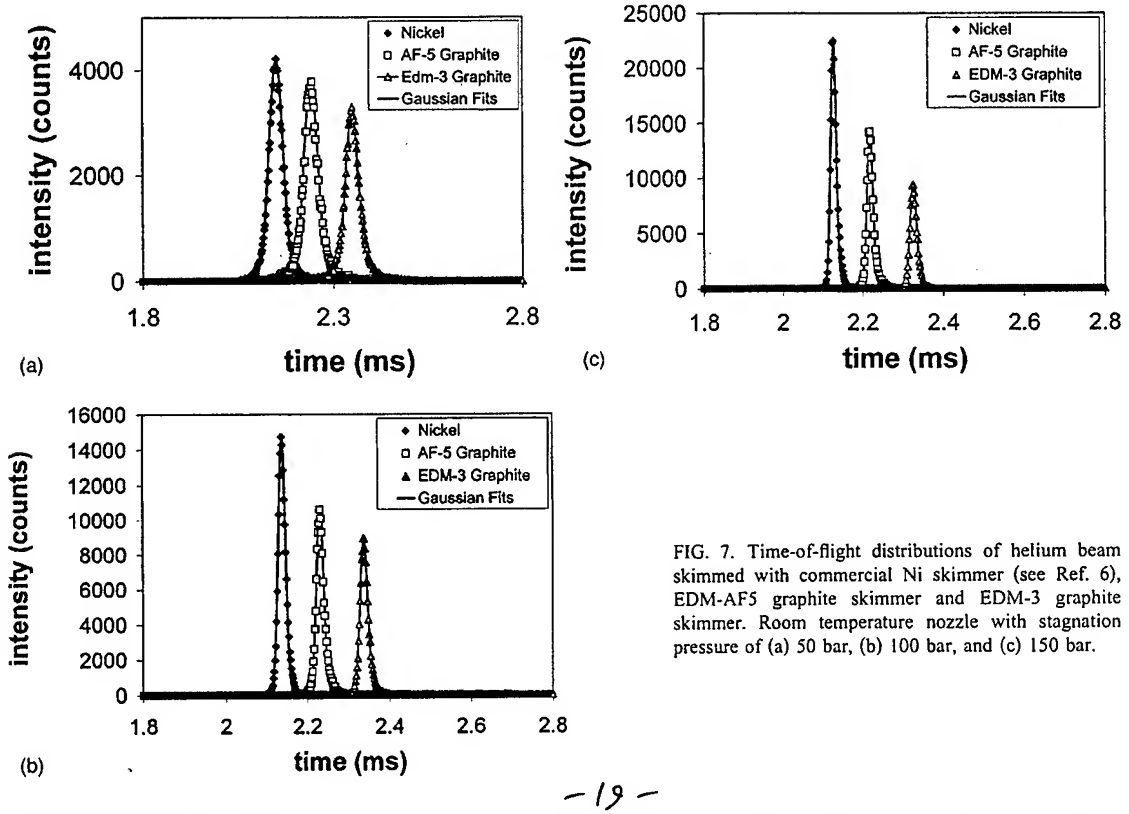


FIG. 7. Time-of-flight distributions of helium beam skimmed with commercial Ni skimmer (see Ref. 6), EDM-AF5 graphite skimmer and EDM-3 graphite skimmer. Room temperature nozzle with stagnation pressure of (a) 50 bar, (b) 100 bar, and (c) 150 bar.

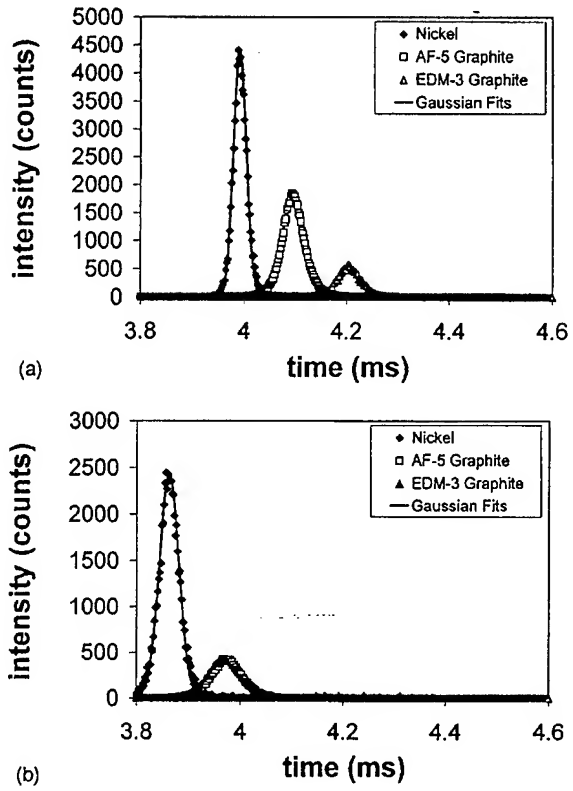


FIG. 8. Time-of-flight distributions of helium beam skimmed with commercial Ni skimmer (see Ref. 6), EDM-AF5 graphite skimmer and EDM-3 graphite skimmer. Liquid-nitrogen-cooled nozzle with stagnation pressure of (a) 50 bar, (b) 100 bar.

bar. A very similar trend is seen in the TOF peak height for the EDM-3 skimmer relative to that for the EDM-AF5 skimmer. These trends indicate the onset of skimmer interference. Under rarefied flow conditions, skimmer interference involves the formation of a low density "cloud" [26] in front of the skimmer as unskimmed atoms backscatter from the leading edge and front surface of the skimmer. The blunter the skimmer, the denser this backscattered cloud, and hence the greater the skimmer interference. If the cloud is relatively low in density, each beam atom undergoes at most a single collision in passing through it. This removes the effected atom from the directed beam, thereby attenuating the beam, but does not alter the velocity distribution of the transmitted beam. At its onset, then, skimmer interference produces moderate intensity attenuation but has little effect on the beam velocity distribution. For the room temperature beam, this is clearly the situation for the graphite skimmers relative to the Ni skimmer (which may, of course, also be experiencing some skimmer interference relative to a "perfect" skimmer).

To affect the velocity distribution of the skimmed beam, it is necessary for a beam atom scattering from the cloud to undergo a second collision and return to the directed beam with an altered velocity. This process should emerge at higher beam intensity. Nozzle throughput scales to first order with $T^{-1/2}$ and is thus expected to double as the nozzle is cooled from room temperature to liquid-nitrogen temperature. In the absence of skimmer interference, the beam intensity would also double and the TOF peak height, a measure of the *spectral* intensity, would increase by an even larger factor as the velocity distribution narrows concomitantly. With the increased throughput, however, comes an increase in backscattering and thereby in cloud density in front of the skimmer. Moreover, the frequency of beam-cloud collisions is inversely proportional to the velocity of both the beam and the cloud atoms and thereby considerably higher for a liquid-nitrogen-cooled beam than for a room temperature beam. In spite of increased throughput with the cold nozzle, therefore, the measured beam intensity can easily drop due to increased skimmer interference. Since skimmer interference is already apparent with the room temperature beam, the interference

TABLE II. Summary of TOF measurements and dc beam measurements for various nozzle stagnation pressure $P_0$ and temperature $T_0$. dc beam intensity was measured both with the quadrupole mass spectrometer beam detector (QMS) and with a pitot chamber. Measurements have been scaled to standard set of experimental settings to allow a direct comparison values within each column.

| | | | TOF beam measurement | | DC beam intensity measurement | |
|---|---|---|---|---|---|---|
| | $T_0$ (K) | $P_0$ (bar) | $\Delta t/t$, FWHM (%) | Peak height (cnts) | QMS detector (cnts/s) | Pitot chamber ($10^{19}$ #/sr/s) |
| Nickel | 300 | 50 | 1.98 | 4214 | 100 000 | 4.95 |
| | 300 | 100 | 0.98 | 14 725 | 170 000 | 6.29 |
| | 300 | 150 | 0.80 | 22 470 | 220 000 | 7.78 |
| | 77 | 50 | 0.74 | 4406 | 70 000 | 4.66 |
| | 77 | 100 | 1.10 | 2446 | 60 000 | 3.41 |
| EDM-AF5 | 300 | 50 | 1.99 | 3779 | 95 000 | 4.47 |
| | 300 | 100 | 0.99 | 10 600 | 130 000 | 6.34 |
| | 300 | 150 | 0.85 | 14 250 | 150 000 | 6.34 |
| | 77 | 50 | 1.24 | 1847 | 50 000 | 2.16 |
| | 77 | 100 | 1.74 | 422 | 16 000 | 0.77 |
| EDM-3 | 300 | 50 | 2.02 | 3301 | 90 000 | 3.41 |
| | 300 | 100 | 1.03 | 8940 | 110 000 | 4.27 |
| | 300 | 150 | 0.91 | 9390 | 100 000 | 4.32 |
| | 77 | 50 | 1.26 | 578 | 17 000 | 1.25 |
| | 77 | 100 | 1.63 | 1 | 900 | 0.29 |

should move into the multiple scattering regime with the colder nozzle, affecting the TOF peak width in addition to the beam intensity. The experimental TOF show exactly these trends. As seen in Fig. 8 and Table II, the TOF peak width for the EDM-AF5 skimmer now substantially exceeds that for the Ni skimmer and likewise for the EDM-5 skimmer relative to the EDM-AF5 skimmer. All TOF peaks heights and widths deteriorate as the source pressure is raised from 50 to 100 bar. Again the deterioration scales with the lip radius of the skimmer. All skimmers are therefore experiencing substantial skimmer interference under these conditions, with the effects most pronounced for the skimmers having larger lip radii.

To our knowledge, this is the first explicit characterization of the effect of skimmer lip radius on the intensity and velocity distribution of a supersonic nozzle beam. It provides dramatic confirmation of the need to use ultrasharp skimmers when operating at extreme beam intensities. It also demonstrates that the graphite skimmers, while useful for high resolution supersonic beam work at room temperature, are not the tool of choice with a liquid-nitrogen-cooled nozzle. On the other hand, the graphite skimmers should function extremely well at temperatures far above room temperature, as is their intended regime of application.

## VI. dc MEASUREMENTS OF BEAM INTENSITY

To complement the TOF peak heights presented above, beam intensities of the unchopped beam were measured both with the quadrupole mass spectrometer detector and, to obtain an absolute calibration, with a pitot chamber. [25] The entrance aperture to the pitot chamber was located 2.92 m downstream of the skimmer apex. The pressure rise within the pitot chamber was measured with a standard Bayard–Alpert ionization gauge and thus the absolute accuracy of those measurements was only as accurate as the gauge calibration (~100%). However, the relative comparison from skimmer to skimmer should be quite accurate (~5%). For each measurement, the source-skimmer distance was varied to optimize the beam intensity and it is those optimized intensities for the direct beam which are tabulated in the final two columns of Table II.

Considerable information on skimmer interference effects are contained within a measurement of beam intensity as a function of source-skimmer distance. Such measurements are shown in Fig. 9 for the room temperature beam and in Fig. 10 for the liquid-nitrogen-cooled beam. Separate plots are presented for different source pressures in both cases. All curves display the same form, namely, a maximum in intensity at a source-skimmer distance of typically 25–30 mm accompanied by a rolloff in intensity at both larger and smaller separations. (As mentioned above, all TOF measurements were made with the nozzle-skimmer distance positioned to yield this maximum intensity.)

The decrease in intensity at small separations is generally ascribed to elevated skimmer interference as the nozzle is placed close to the skimmer. [3] Increasing the lip radius of the skimmer and thereby worsening skimmer interference should move the onset of this rolloff to larger separations. The experimental data show exactly this trend, with the rolloff occurring at increasing nozzle-skimmer distances in the order Ni skimmer, EDM-AF5 skimmer, EDM-3 skimmer. The data are thus entirely consistent with the interpre-

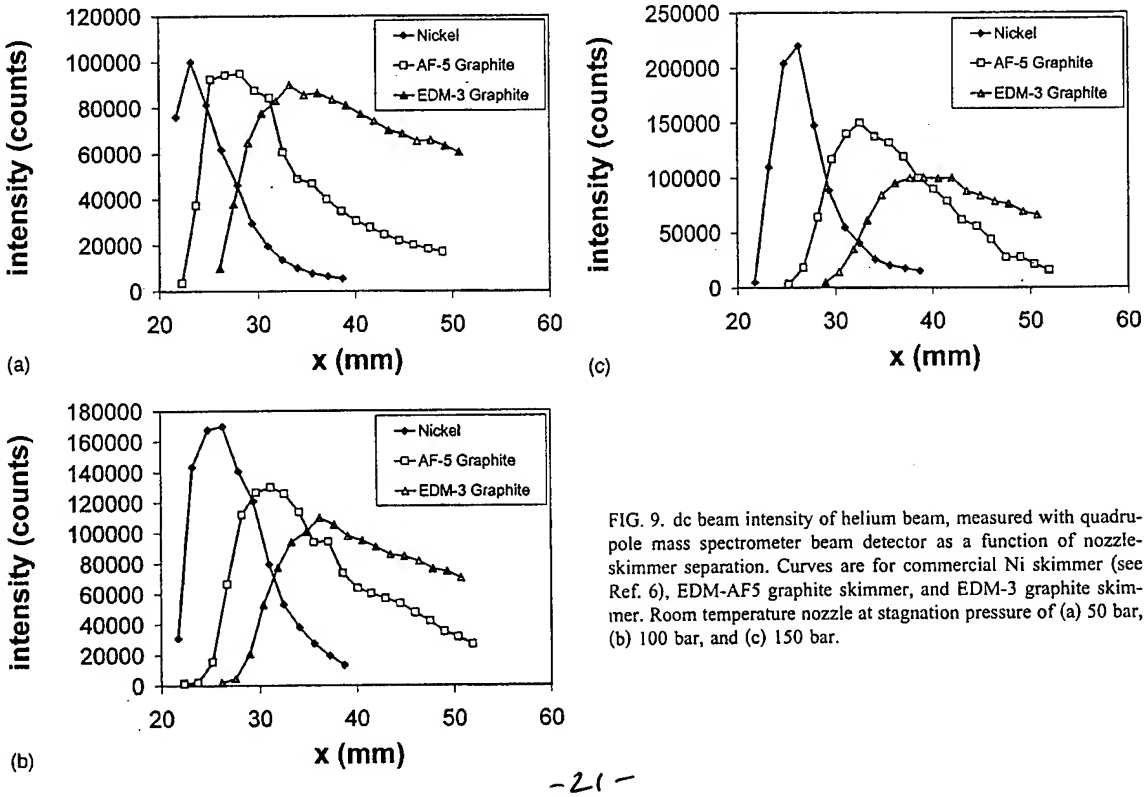


FIG. 9. dc beam intensity of helium beam, measured with quadrupole mass spectrometer beam detector as a function of nozzle-skimmer separation. Curves are for commercial Ni skimmer (see Ref. 6), EDM-AF5 graphite skimmer, and EDM-3 graphite skimmer. Room temperature nozzle at stagnation pressure of (a) 50 bar, (b) 100 bar, and (c) 150 bar.

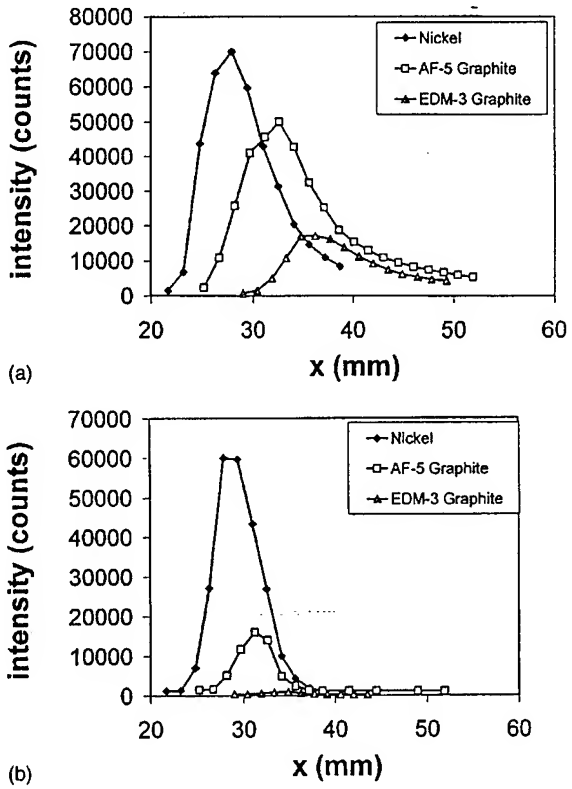


FIG. 10. dc beam intensity of helium beam, measured with quadrupole mass spectrometer beam detector as a function of nozzle-skimmer separation. Curves are for commercial Ni skimmer (see Ref. 6), EDM-AF5 graphite skimmer, and EDM-3 graphite skimmer. Liquid-nitrogen-cooled nozzle at stagnation pressure of (a) 50 bar and (b) 100 bar.

tation of increasing skimmer interference as the nozzle is brought closer to the skimmer.

The rolloff in beam intensity at large separations would normally be explained as simple Beer's Law attenuation of the beam by the ambient background in the source chamber. Were that the case, however, the curves for all three skimmers should approach a single limiting curve at large nozzle-skimmer separations since it is only the skimmer characteristics which are being varied, the nozzle parameters being held unchanged within each data set.

Accordingly, we must conclude that skimmer properties play a substantial role even at very large nozzle-skimmer separations of 40 mm. Particularly striking is that the "worse" skimmers outperform the "better" skimmers substantially at these large separations. This might be partly due to the somewhat different geometries. The commercial Ni skimmer has a slightly smaller diameter (0.50 mm) than the EDM-AF5 (0.80 mm) and the EDM-3 (0.75 mm) and this is known to influence beam characteristics.[27] In addition, the sidewall angle of the Ni skimmer increased from apex to base, providing additional area relief within the nozzle, whereas the graphite skimmers had straight conical sidewalls as shown in Fig. 1. Such geometrical differences can affect not only the expansion within the skimmer but may also influence the boundary layer formation and standoff at the endwall.[3,27] It should be noted that the curves for the EDM-3 skimmer vary little as the source pressure is raised, while the maxima in the curves for both the EDM-AF5 and Ni skimmers increase with increasing pressure. Additional insight may come from the measurements with the liquid-nitrogen-cooled nozzle: Under these conditions, known from the TOF measurements to produce substantial skimmer interference, the curves for the three skimmers do indeed seem to more nearly approach a single limiting curve at large nozzle-skimmer separations. We are currently unable to explain these trends with the room temperature nozzle, other than to postulate that the critical parameter in setting beam intensity is the total gas density, beam *plus* cloud, at the mouth of the skimmer.

## VII. DISCUSSION

EDM graphite offers a useful material for molecular beam skimmers. Skimmers fabricated from Poco grade EDM-AF5 perform aerodynamically nearly as well as the best commercial skimmers, are much less expensive, and are refractory. The EDM skimmers thus provide a means of skimming free-jets which are corrosive, energetic, or electronically highly excited. Of particular, relevance is the application of these EDM skimmers to extract or collimate a plasma discharge.

Ancillary to the principal objective of characterizing these skimmers, our TOF and beam intensity measurements offer insight into the effect on skimmer interference of the lip radius of the skimmer knife edge. Substantial interference effects are observed and correlated with increasing bluntness of the skimmer knife edge, but not yet fully understood.

[1] D. R. Miller, in *Atomic and Molecular Beam Methods, Vol. I*, edited by G. Scoles (Oxford University Press, Oxford, 1988), pp. 14–53.
[2] U. Bossel, Entropie **42**, 12 (1971).
[3] U. Bossel, F. C. Hurlbut, and F. S. Sherman, in *Rarefied Gas Dynamics, Vol. II*, edited by L. Trilling and H. Y. Wachman (Academic, New York, 1969), pp. 945–964.
[4] *Atomic and Molecular Beam Methods, Vol. I & II*, edited by G. Scoles (Oxford University Press, Oxford, 1988).
[5] W. R. Gentry and C. F. Giese, Rev. Sci. Instrum. **46**, 104 (1975).
[6] Beam Dynamics, Inc., 708 East 56th Street, Minneapolis, MN 55417.
[7] W. S. Young, W. E. Rodgers, and E. L. Knuth, Rev. Sci. Instrum. **40**, 1346 (1969).
[8] R. W. Bickes, Jr., K. R. Newton, J. M. Harrington, and R. B. Bernstein, J. Chem. Phys. **64**, 3648 (1976).
[9] K. R. Way, S.-C. Yang, and W. C. Stwalley, Rev. Sci. Instrum. **47**, 1049 (1976).
[10] S. J. Sibener, R. J. Buss, C. Y. Ng, and Y. T. Lee, Rev. Sci. Instrum. **51**, 167 (1980).
[11] H. Ferkel, R. Feltgen, and D. Pikorz, Rev. Sci. Instrum. **62**, 2626 (1991).
[12] Maryland Lava Company, Inc., P.O. Box 527, Bel Air, MD 21014.
[13] A. Lebéhot and R. Campargue, Phys. Plasmas **3**, 2502 (1996).
[14] F. J. Grunthaner, Proceedings of the 45th International Symposium of American Vacuum Society, Baltimore, MD, 2–6 November 1998.
[15] S. Nowak, T. Pfau, and J. Mlynek, Appl. Phys. B: Lasers Opt. **63**, 203 (1996).
[16] J.-Y. Loo, J. D. Lobo, S. Blumberg, T. S. Dibble, X. Zhang, C.-C. Tsao, and M. Okamura, J. Appl. Phys. **81**, 5896 (1997).
[17] H. S. Niu, K. Hu, and R. S. Houk, Spectrochim. Acta B **46**, 806 (1991).
[18] M. A. Cappelli, A. E. Kul, K. Schwendner, H. Lee, S. J. Harris, Jr., and J. Mroczkowski, Mater. Res. Soc. Symp. Proc. **423**, 359 (1996).
[19] H. P. Gillis, D. A. Choutov, K. P. Martin, and S. Li, Appl. Phys. Lett. **68**, 2255 (1996).
[20] J. J. Valentini, M. J. Coggiola, and Y. T. Lee, Rev. Sci. Instrum. **48**, 58 (1977).
[21] J. J. Valentini (private communication).

[22] Poco Graphite, Inc. 1601 S. State Street, Decatur TX 76234. Internet address http://www.poco.com.
[23] Thermal Machining Processes, Society of Manufacturing Engineers, Dearborn MI, 1979, ISBN 0-87263-049-8.
[24] M. Kandah and J.-L. Meunier, IEEE Trans. Plasma Sci. **24**, 523 (1996).
[25] R. B. Doak, in *Atomic and Molecular Beam Methods, Vol. II*, edited by G. Scoles (Oxford, New York, 1992).
[26] *Molecular Beams and Low Density Gasdynamics*, edited by P. P. Wegener (Dekker, New York, 1974), p. 51 ff.
[27] R. Campargue, J. Phys. Chem. **88**, 4466 (1984).

## IV. CORONA DISCHARGE SUPERSONIC FREE-JET (CD-SFJ)

Following theoretical predictions that the $A^3\Sigma_u^+$ molecular nitrogen (the lowest triplet metastable state of molecular nitrogen) should be preferable to atomic nitrogen for III-N growth, the research effort was shifted to corona discharge supersonic free-jets (CD-SFJ). Both positive and negative CD-SFJ's were investigated as to their selective production of $A^3\Sigma_u^+$ in the absence of more energetic and detrimental activation states of N and $N_2$. The $A^3\Sigma_u^+$ yield of both polarities was similar and was low in terms of absolute flux. Positive CD-SFJ's always yielded nitrogen ions, making them unsuitable for III-N growth. With considerable effort, the $A^3\Sigma_u^+$ yield was coaxed from a beam fraction of initially only 0.1% up to nearly 2%. While still modest for commercial applications, this sufficed for experimental growth of thin GaN and AlN films for the purpose of characterizing the growth process. The activation state analysis of the CD-SFJ was made using Appearance Potential Spectroscopy (APS), in which the electron bombardment ionization yield is measured as a function of the electron impact energy. Electronically excited states have a lower threshold for ionization, and this provides a signature by which to identify them. The following paper, "Corona Discharge Supersonic Free-Jet for III-V Nitride Growth via $A^3\Sigma_u^+$ Metastable Nitrogen Molecules," D.C. Jordan, C. Burns, R.B. Doak, J. Appl. Phys. **89**, 883-892, (2001), provides details on the CD-SFJ characterization.

# Corona discharge supersonic free-jet for III–V nitride growth via $A\,^3\Sigma_u^+$ metastable nitrogen molecules

D. C. Jordan,[a] C. T. Burns,[b] and R. B. Doak[c]
*Department of Physics and Astronomy, Arizona State University, Tempe, Arizona 85287-1504*

(Received 22 May 2000; accepted for publication 16 October 2000 )

A corona discharge supersonic free-jet is shown to be a nearly pure source of $A\,^3\Sigma_u^+$ metastable molecular nitrogen, an electronically excited and chemically active form of $N_2$ that is ideally suited to nitride semiconductor growth. Optical emission spectroscopy at various distances downstream of the supersonic nozzle reveals a cascade through the excited state manifold of $N_2$ triplet states to populate the $A\,^3\Sigma_u^+$ state. Appearance potential spectroscopy (mass spectrometer electron bombardment ionization yield, measured as a function of electron impact energy ) delivers the composition of the terminal molecular beam. $A\,^3\Sigma_u^+$ molecules are the dominant activated species in the beam, which otherwise contains only nonreactive $X\,^1\Sigma_g^+$ ground state nitrogen molecules plus a minor amount of $^4S^0$ nitrogen atoms. Up to 1.56% number fraction of the beam is $A\,^3\Sigma_u^+$, providing $1.0\times10^{17}$ metastables $sr^{-1}\,s^{-1}$. © *2001 American Institute of Physics.*
[DOI: 10.1063/1.1331646]

## I. METASTABLE MOLECULAR NITROGEN FOR III–N GROWTH

AlN, GaN, and InN have emerged as materials of choice for wideband gap semiconductor devices.[1,2] Despite remarkable advances in III–N fabrication in recent years, better understanding and further optimization of growth processes remain goals. It has been calculated[3] that $A\,^3\Sigma_u^+$ metastable molecular nitrogen should be an ideal precursor for molecular beam epitaxy (MBE) of III–N materials. This electronically excited state couples to the ground state solely via the forbidden Vegard–Kaplan bands. It therefore has a very long lifetime, ~1 s, exceeding by many orders of magnitude any molecular beam transit time through an MBE apparatus. Consequently, metastable $A\,^3\Sigma_u^+$ molecules can be employed in much the same fashion of any stable MBE species. The suggested use of $A\,^3\Sigma_u^+$ to grow III–N nitrides[3] is based on two facts: (1) Being electronically excited, $A\,^3\Sigma_u^+$ is chemically reactive ("activated"). (2) Being molecular rather than atomic, $A\,^3\Sigma_u^+$ delivers two atoms simultaneously to the surface. In the ensuing dissociative chemisorption reaction, one of these atoms can bind to the surface while the second carries away the heat of reaction as kinetic energy. Consequently the reaction exothermicity need not be dissipated through the III–N film. Nitrogen accommodation is enhanced and sputtering damage minimized, improving film quality.

Various electrical discharges are employed to "activate" nitrogen, including radio frequency (rf) discharges,[4,5] microwave discharges,[6] electron cyclotron resonance (ECR) discharges,[7–9] arc-jet discharges,[10,11] and hollow anode plasma discharges.[12] These discharges often yield $A\,^3\Sigma_u^+$, but are invariably accompanied by numerous other electronically excited states of nitrogen atoms, molecules, and even ions. In contrast, as is shown herein, a corona discharge supersonic free-jet (CDSFJ) can produce a beam containing essentially only the $A\,^3\Sigma_u^+$ activation state. This article provides a detailed characterization of the CDSFJ as a source of $A\,^3\Sigma_u^+$ nitrogen. Actual growth of III–N thin films with the CDSFJ source is discussed elsewhere, including measurement of the $A\,^3\Sigma_u^+$ incorporation efficiency[13,14] and description of the film morphologies obtained under various growth conditions.[13]

## II. CORONA DISCHARGE SUPERSONIC FREE-JET SOURCES

Apart from its very high initial gas temperature (several thousand degrees), a CDSFJ is similar to any supersonic free-jet.[15] Its state specificity derives from very rapid cooling within the free-jet expansion. The corona discharge is struck within the supersonic nozzle, upstream of the nozzle throat, to heat and excite the nitrogen gas. As the gas expands through the throat into high vacuum, the free-jet density decreases rapidly and this causes the discharge to terminate within a few nozzle diameters.[16] The expansion itself continues much farther downstream, depopulating excited states both by collision-induced relaxation within the continuum expansion itself and by spontaneous radiative relaxation in the subsequent free molecular flow.[17] With proper selection of discharge parameters (discharge power, corona polarity, nozzle stagnation pressure, and nozzle diameter ), all but very long-lived species return to the ground state. The manifold of $N_2$ triplet excited states cascades down to collect in the metastable $A\,^3\Sigma_u^+$ state and this survives as the dominant reactive form of nitrogen in an otherwise essentially ground state, nonreactive beam.

[a]Current address: Department of Electrical Engineering, Arizona State University, Tempe, AZ 85287.
[b]Current address: Department of Electrical and Computer Engineering, University of California, Santa Barbara, CA.
[c]Electronic mail: bdoak@asu.edu

 

TABLE I. Top two rows: Maximum integral cross sections for excitation of relevant $N_2$ species; electron impact voltage at which maximum occurs (Ref. 52). Following rows: Representative radiative lifetimes of species in various vibrational levels.

| Excited species | $A\,^3\Sigma_u^+$ | $B\,^3\Pi_g$ | $C\,^3\Pi_u$ | $W\,^3\Delta_u$ |
|---|---|---|---|---|
| Maximum excitation cross section | 0.225 Å$^2$ | 0.299 Å$^2$ | 0.443 Å$^2$ | 0.380 Å$^2$ |
| Electron impact voltage | 17 V | 12 V | 14 V | 16 V |
| Radiative lifetime | | | | |
| $v=0$ | 1.3\2.5 s | 8–13 $\mu$s | 36–39 ns | 4\32 s |
| $v=1$ | 1.3 s | 8–11 $\mu$s | 36–39 ns | 4.5 ms |
| $v=2$ | 1.3 s | 7–9 $\mu$s | 37–38 ns | 1.2 ms |
| $v=3$ | 1.4 s | 7–8 $\mu$s | 38 ns | 600 $\mu$s |
| $v=4$ | 1.4 s | 6–7 $\mu$s | 36–39 ns | 370 $\mu$s |
| $v=8$ | 1.4 s | 5 $\mu$s | — — — | 130 $\mu$s |
| References, radiative lifetimes | 53 | 54 | 54 | 17, 55 |

CDSFJ production of metastable species dates to seminal work with rare gases by Searcy.[18] The technique was subsequently developed by Leasure *et al.*[19] and by Fahey and coworkers.[20,21] The latter reported beam intensities of $3.5\times10^{14}$, $1.5\times10^{14}$, and $7.2\times10^{13}$ metastables sr$^{-1}$ s$^{-1}$ with helium, neon, and argon, respectively. CDSFJ expansions have been used extensively to produce cold radicals for spectroscopic analysis[22,16,23,24] and such work has included nitrogen.[25,26] However, since spectroscopic measurements require neither a single excited state nor exceptional quantities of that state, the metastable flux and state purity of nitrogen CDSFJ beams has rarely been examined. An exception is the CDSFJ variant of Neuschäfer *et al.*,[17] who struck a corona discharge between their nozzle and skimmer to yield $A\,^3\Sigma_u^+$ fluxes of $5\times10^{+13}$ metastables cm$^{-2}$ s$^{-1}$ at 50 cm from the nozzle. That source also yielded $W\,^3\Delta_u$ at about 10% of the $A\,^3\Sigma_u^+$ density plus minor amounts of $E_3\Sigma_g^+$, $a\,^1\Pi_g$, and Rydberg states.

Relevant excited species in a CDSFJ of nitrogen are the $N_2$ triplet states $A\,^3\Sigma_u^+$, $B\,^3\Pi_g$, $C\,^3\Pi_u$, and $W\,^3\Delta_u$. Other excited states may also be present, but play no significant role due to small excitation cross sections and/or short lifetimes.[17] Electron impact excitation cross sections for the triplet states are listed in Table I along with radiative lifetimes for representative vibrational levels. The terminal beam velocity for a pure nitrogen CDSFJ is typically ~2000 m/s. At this speed and given the lifetimes of Table I, the $A\,^3\Sigma_u^+$ state would survive for kilometers, the $W\,^3\Delta_u$ for meters, the $B\,^3\Pi_g$ state for centimeters, and the $C\,^3\Pi_u$ state for only microns. Reexcitation can alter these trends. In particular, the $W\,^3\Delta_u$ vibrational levels overlap with those of the $A\,^3\Sigma_u^+$ and $B\,^3\Pi_g$ and relax via a cascade through the latter states, repopulating the $B\,^3\Pi_g$ states and giving rise to a long-lived afterglow on the $B\rightarrow A$ emission lines.[17] Thus a CDSFJ nitrogen molecular beam might conceivably contain not just $A\,^3\Sigma_u^+$ but also lower vibrational levels of $W\,^3\Delta_u$ and (transiently) $B\,^3\Pi_g$. The exact composition can only be determined through experimental measurement. Any such characterization is complicated by the fact that $A\,^3\Sigma_u^+$ is truly metastable and therefore nonemitting.

## III. EXPERIMENTAL MEASUREMENTS AND APPARATUS

In this work, the nitrogen CDSFJ was probed via (1) optical spectroscopy to characterize electronic relaxation within the free-jet expansion, (2) time-of-flight (TOF) measurements of the beam velocity and velocity spread,[27] (3) stagnation pressure gauge ("pitot") measurements of beam flux, and (4) appearance potential spectroscopy (APS) measurements of the relative beam composition. Beams of 100% nitrogen were investigated, as were mixtures of 10% and 20% mole fraction $N_2$ in Ar. For all mixtures, measurements were made with the corona wire operated both as an anode (positive) and as a cathode (negative) with respect to a grounded electrode surrounding the nozzle. These are referred to below as "positive" and "negative" corona discharges, respectively.

The corona discharge free-jet source, depicted schematically in Fig. 1, was similar to those described in the literature.[18–23] It consisted of a quartz tube (6 mm o.d., 4 mm i.d.), heated and drawn to closure then ground back to form a nozzle orifice diameter of 200 $\mu$m as measured by an optical comparator. The nozzle tube was mounted in a 1/4 in. Swagelock cross to allow a 0.25 mm diameter tungsten or rhenium corona wire to be inserted via a high voltage feedthrough welded into the opposing leg of the cross. Source gas entered through one transverse leg and the opposing leg served to mount the cross on a 1/4 in. stub within the source vacuum chamber. The nozzle was operated at a stagnation pressure of 200–440 Torr, producing a background pressure of typically $1\times10^{-6}$ Torr in a source vacuum chamber pumped by an 18 000 l/s diffusion pump. A grounded cylindrical electrode, mentioned above, surrounded the nozzle tube outside of the free-jet boundary to provide a point of attachment for the corona. Application of 4–6 kV to the

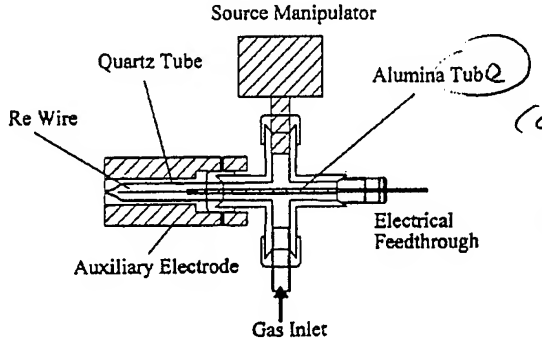


FIG. 1. Schematic depiction of the supersonic corona discharge source.

TABLE II. Measured values of mean velocity, velocity spread, and mean energy for CDSFJ expansions of various gas mixtures, polarities, and input power. The quoted beam intensities are total $N_2$ flux, including both excited and ground state species.

| Gas | Polarity | Pressure (Torr) | Current (mA) | Mean velocity (m/s) | Velocity spread (FWHM, %) | Mean energy (eV) | Total beam intensity ($10^{18}$ $N_2$/sr/s) |
|---|---|---|---|---|---|---|---|
| 100% $N_2$ | Neg. | 482 | 18 | 2064 | 24.7 | 0.62 | 6.47 |
| | Neg. | 450 | 9.6 | 1937 | 31.1 | 0.54 | 5.71 |
| | Neg. | 440 | 7.5 | 1796 | 24.3 | 0.47 | 5.49 |
| | Pos. | 425 | 6 | 1868 | 23.3 | 0.50 | 5.58 |
| 20% $N_2$ | Neg. | 790 | 18 | 1571 | 13.1 | 0.36 | 0.60 |
| | Neg. | 440 | 7.5 | 1285 | 14.9 | 0.24 | 0.45 |
| | Pos. | 440 | 7.3 | 1216 | 14.1 | 0.21 | 0.41 |
| 10% $N_2$ | Neg. | 440 | 7.5 | 1189 | 10.6 | 0.20 | 0.34 |
| | Pos. | 455 | 8 | 1173 | 9.5 | 0.20 | 0.39 |

corona wire through a 250 kΩ series ballast resistor[16] produced a discharge current of 6–18 mA and resulted in a readily discernible bright plume at the tip of the nozzle. The turn-on procedure was as follows. (1) The gas pressure in the nozzle was raised to the desired value. (2) The current limit of the high voltage power supply was set to the desired discharge current. (3) The voltage was raised until the discharge initiated. This produced a jump in current, placing the power supply into current-limited mode. The emission current could then be adjusted within bounds set by the electrical characteristics of the corona discharge.[13]

A few centimeters downstream of the nozzle, a custom-made 0.75 mm diameter refractory graphite skimmer[28] extracted the isentropic core of the free-jet plasma expansion to form the molecular beam. Several differentially pumped vacuum chambers led to a deposition chamber where controlled growth took place under UHV conditions, 0.64 m from the nozzle exit. An Extrel Model 7-324-9 quadrupole mass spectrometer detector viewed the incident beam at a distance of 3.96 m from the source. Appearance potential spectroscopy (APS) was carried out by recording the detector signal while varying the electron impact ionization energy. A chopper disk just downstream of the skimmer pulsed the beam for time-of-flight energy analysis over a chopper-detector distance of 3.76 m. The chopper also served as a beam flag, allowing the dc background of the APS spectra to be determined and subtracted. Calibrated, absolute measurements of the beam flux were made using the pitot chamber, the entrance aperture to which was 2.81 m from the skimmer apex. A residual gas analyzer in the pitot chamber allowed separate flux measurements of all components of a mixed gas beam.

An optical monochromator viewed the beam transversely to the beam axis through a fused silica window in the nozzle chamber wall, permitting spectroscopic measurements of the corona plume at any position from the nozzle exit up to several centimeters downstream. A 1 in. diameter fused silica f/4 lens focused the image of the plasma plume onto the 100 $\mu$m wide slit of a 0.5 m Jarrell-Ash monochromator, the output of which was detected by a R446 Hamamatsu photomultiplier tube (PMT), amplified, then read into a data acquisition board of a laboratory PC computer.

### A. Time of flight (TOF) beam measurements

Measurements of the beam velocity, velocity spread, and energy are summarized in Table II for various source conditions. As seen from the first three rows, the velocity and the kinetic energy increase with increasing discharge current for a negative corona. The shift is small, however, with respect to the velocity distribution, which was broad at all beam compositions due to the low source pressure and high temperature of the discharge. Pure nitrogen beams had a broader velocity distribution than did $N_2$/Ar mixtures. At any given discharge current, a slightly more energetic beam was obtained for the positive corona than for the negative corona and this was attributed to the presence of energetic streamers within the positive discharge as described below. The data of Table II show manifestly different velocity characteristics for the negative and the positive corona discharges of pure nitrogen. These differences diminished as nitrogen concentration was lowered, to the point that both polarities yielded essentially identical velocity distributions with 10% mole fraction of nitrogen in argon. Measurements under constant discharge conditions while varying the $N_2$/Ar ratio revealed the dominant effect of argon to be a deceleration of the nitrogen molecules, as expected from the gas dynamics of seeded beams.[29] This deceleration increased as the beam fraction of $N_2$ decreased, as did a small but distinct velocity slip of the argon relative to the nitrogen.

### B. Pitot measurements of absolute beam intensity

The pitot vacuum chamber could be closed off from all pumps and vacuum connections apart from a single aperture of known area on the beam axis, which was fully filled by the incoming beam. The directed, incoming beam flux through this aperture is randomized by wall collisions, raising the pressure within the pitot chamber until the beam influx is exactly balanced by free molecular outflow through the orifice, whereupon the pressure rise in the chamber is easily and exactly related to the incoming beam flux. The

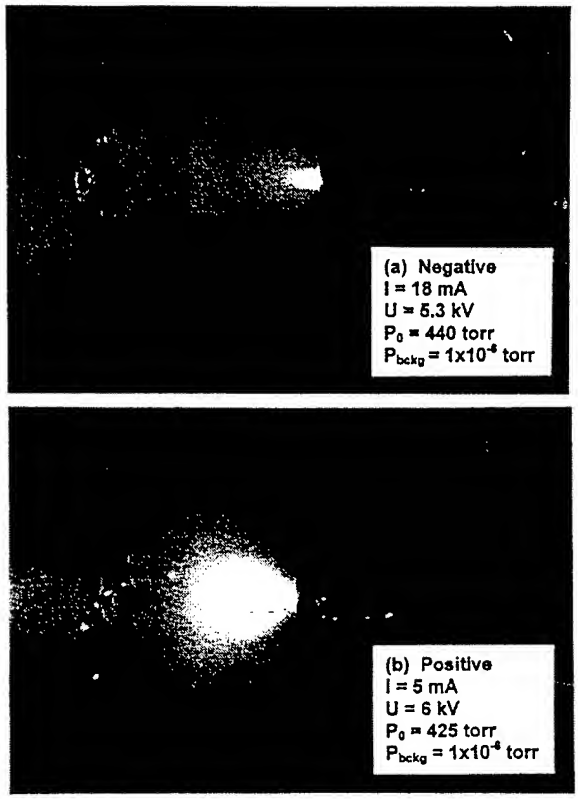


FIG. 2. Photos of the 100% nitrogen CDSFJ for (a) negative and (b) positive corona tip Ref. 30. Nozzle and discharge parameters are provided in the insets. The bright spots seen only with positive corona and not with the negative are streamer attachment points to ground at the chamber wall or at the cylindrical electrode surrounding the nozzle tube. The 1 in. high conical graphite skimmer is visible at the left of each picture. The source has been retracted from the skimmer to facilitate the photography, the source-skimmer distance being about 30 cm in normal operation.

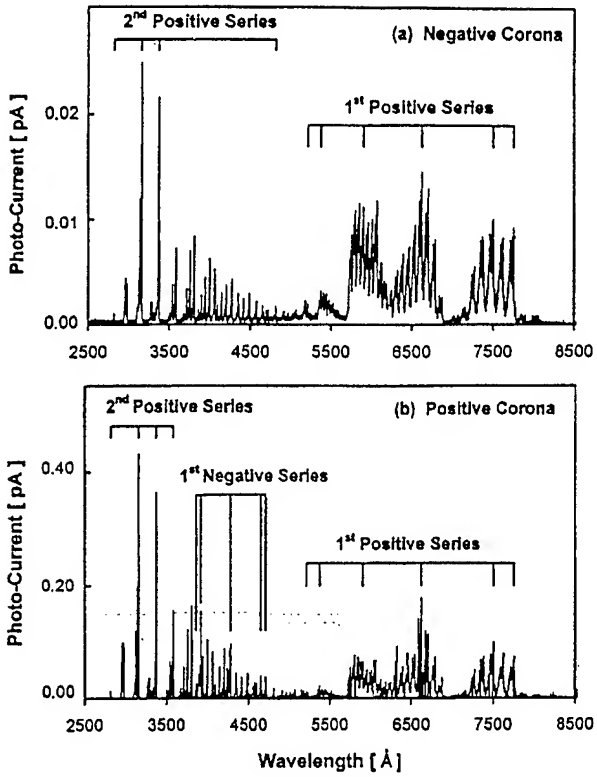


FIG. 3. Optical emission spectra measured at the nozzle exit for (a) negative and (b) positive corona discharges in a CDSFJ beam of 100% nitrogen. Vertical bars mark tabulated wavelengths of specific strong emission lines (Refs. 37 and 57).

pressure was measured with a standard Bayert–Alpert ionization gauge, calibrated against a National Institute of Standards and Technology-traceable calibrated leak. Measured, absolute beam intensities for various discharge settings are compiled in Table II. A total beam intensity of 6 $\times 10^{18}$ molecules $sr^{-1}$ $s^{-1}$ was routinely obtained for a CDSFJ of 100% nitrogen.

### C. Optical emission spectroscopy measurements

Photographs of typical corona discharge plumes are provided in Fig. 2. The appearance depended strongly on the polarity of the corona wire relative to the circular guard electrode surounding the nozzle. The positive corona developed a bright purple-violet plasma plume whereas the negative corona plume was orange and less luminous.[30] The positive corona was interrupted by continual flickering and sparking while the negative discharge was steady and stable. The positive corona discharge ran at lower discharge current but somewhat higher voltage than the negative corona.

Optical emission spectra were recorded for a wide variety of beam compositions and discharge settings at positions 0, 1, and 3 cm downstream of the nozzle exit.[13] Typical spectra at the exit (0 cm) for negative and positive CDSFJ plumes of 100% nitrogen are presented in Figs. 3 (a) and 3(b), respectively. Emission from neutral molecular nitrogen dominates the spectra, specifically the second positive series ($C\,^3\Pi_u \rightarrow B\,^3\Pi_g$, denoted "2+") and the first positive series ($B\,^3\Pi_g \rightarrow A\,^3\Sigma_u^+$, denoted "1+"). Emission from $N_2^+$ ions, the first negative series (denoted "1−"), is also observed, but only with the positive corona and not with the negative corona. Summing over individual lines within each series, the dependence of 1+, 2+, and 1− emission upon distance from the nozzle is plotted as in Figs. 4 (a) and 4(b). Emission from all series is seen to decrease rapidly with distance from the nozzle. The decline does not scale with either density or collision frequency within the supersonic expansion, since the beam density decreases by over two orders of magnitude within the first few millimeters [13,29] whereas the observed decline in emission is much more protracted. The free-jet expansion undergoes a transition from continuum to free molecular flow less than 1 mm downstream of the nozzle throat.[29,13] Accordingly, the spectroscopy at 1 and 3 cm samples collisionless free molecular flow. The beam also attains its terminal velocity well before reaching the 1 cm point.

Considering first the negative corona and assuming a simple exponential decay in emission intensity, the data of Fig. 4(a) at 1 and 3 cm yield a spatial decay constant of 1.9 cm for the 1+ series of the 100% nitrogen beam. Using the 2064 m/s terminal velocity of the beam, this converts into a temporal decay constant of 9.3 $\mu$s, in excellent agreement

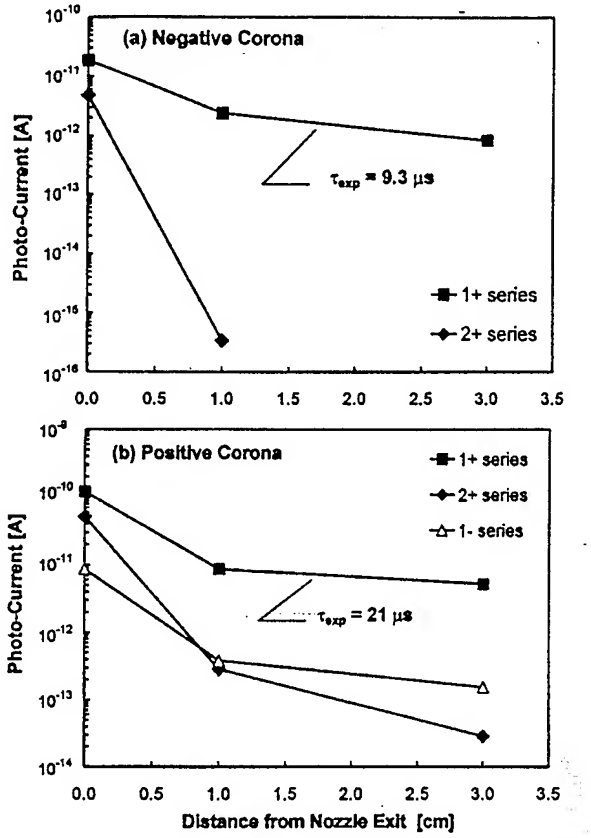


FIG. 4. Integrated spectral intensities for major optical series (see text) for (a) negative and (b) positive CDSFJ beams of 100% nitrogen measured at 0, 1, and 3 cm downstream of the nozzle exit. Experimental decay constants for the $B\,^3\Pi_g$ (1+series) emission were obtained by fitting an exponential decay to data points at 1 and 3 cm, yielding 9.3 and 21 $\mu$s, respectively, for the negative and positive discharges.

with reported lifetimes of the $B\,^3\Pi_g$ state (8–13 $\mu$s, Table I). Thus this 1+ emission of the negative corona between 1 and 3 cm clearly arises through spontaneous relaxation of the $B\,^3\Pi_g$ state. Its more rapid intensity decrease between 0 and 1 cm may reflect collisional deexcitation in the continuum flow regime of the free-jet expansion. The intensity of the 2+ series, which precedes the 1+ series in the relaxation through the $N_2$ triplet manifold, drops much more precipitously between 0 and 1 cm and has disappeared entirely by 3 cm. This reflects the much shorter $C\,^3\Pi_u$ lifetime. Fitting an exponential curve to the intensity at the nozzle exit (0 cm) and at 1 cm downstream, a decay time of 500 ns is extracted for the 2+ series. This is considerably larger than the actual ~40 ns lifetime (Table I), manifesting the fact that transition from continuum to free molecular occurs between these two points, invalidating the model of simple exponential relaxation.

Emission intensity data for the positive corona are presented in Fig. 4(b). One notable difference is the presence of the 1− series of $N_2^+$, which is entirely absent in the negative corona. This $N_2^+$ emission persisted into the free-molecular flow regime, indicating that $N_2^+$ ions survive even into the terminal beam of the positive corona. Production of ions is likely related to streamers,[31–34] which were present in the positive but not the negative corona, as evidenced by bright streamer attachment points seen in the former case [Fig. 2(b)] but not in the latter [Fig. 2(a)]. A second major difference was the much less rapid decline of both 1+ and 2+ emission in the positive corona. A simple exponential fit between 1 and 3 cm yields a decay constant of 21 $\mu$s for 1+ emission from the positive corona, or twice the corresponding value for the negative corona. Accordingly, it appears that both $B\,^3\Pi_g$ and the $C\,^3\Pi_u$ states are replenished within the positive corona free-jet, even in the region of free-molecular flow. Over 5 eV per molecule must be delivered to reexcite these states and accelerated $N_2^+$ ions are probably responsible.

### D. Appearance potential spectra

Excited $N_2$ molecules relaxing via the 2+ and 1+ series must ultimately populate the desired $A\,^3\Sigma_u^+$ metastable state. Emission spectroscopy clearly reveals the cascade, but cannot provide a direct measurement of the $A\,^3\Sigma_u^+$ end state, which does not emit. Accordingly, appearance potential spectroscopy was employed to determine the terminal beam composition. Any electronically excited state has a lower minimum energy for ionization than does the ground state. This manifests itself as a lower threshold in the ionization yield measured as a function of electron bombardment ionization energy, the APS spectrum, and provides a means of identifying even nonemitting states. In the case of molecular nitrogen, both nondissociative and dissociative ionization must be considered, appearing in the mass spectra at mass-to-charge ratios of $m/e=28$ and $m/e=14$, respectively. The overall $A\,^3\Sigma_u^+$ metastable content of the beam is obtained by summing the $A\,^3\Sigma_u^+$ content of these two signals, scaling by the relative ionization yield of the two channels. A fragmentation factor is needed and this was taken from the measured ratio 4.3% for the $m/e=14$ to $m/e=28$ peak heights at an electron impact energy of 45 eV. Although the $m/e=14$ peak is small, its APS spectrum was carefully investigated, not just to establish the exact $A\,^3\Sigma_u^+$ content of the beam but also to gauge the possible presence of atomic nitrogen, which also contributes to this peak.

Provided the ionization cross sections of all contributing states are known, a very accurate assessment of the beam composition can be made from the APS spectra. The overall detector count rate $\dot{N}(E)$ at an electron bombardment energy $E$ is the sum of the count rates due to each contributing species $i$ of density $n_i$ and electron ionization cross section $\sigma_i(E)$,

$$\dot{N}(E)=\sum_i Cj_eV_dn_i\sigma_i(E),$$

where $C$ is an instrumental constant, $j_e$ is the ionization current in the detector, and $V_d$ is the volume of the ionization region. Rewriting this as

$$\dot{N}(E)=\sum_i \alpha_i\sigma_i(E),$$

with $\alpha_i=Cj_eV_dn_i$, it is clear that the APS curve $\dot{N}(E)$ may be fitted by summing the known absolute electron impact

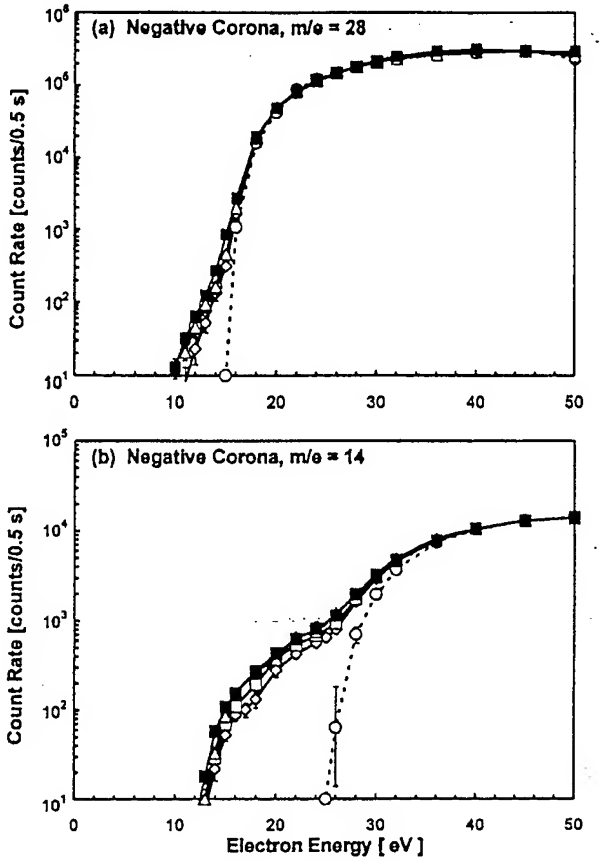


FIG. 5. Appearance potential spectra for a negative corona CDSFJ beam of 100% nitrogen. Spectra are shown for charge-to-mass ratios of (a) $m/e = 28$ and (b) $m/e = 14$, corresponding to the nondissociative and dissociative ionization channels of molecular nitrogen. The symbols mark different discharge currents: no discharge (circles), 8 mA (diamonds), 11 mA (open squares), 14 mA (triangles), and 18 mA (closed squares).

ionization cross sections $\sigma_i(E)$ of the contributing species and scaling each individual ionization cross section curve by a factor $\alpha_i$. The density relative to some chosen species $n_0$ is then given by the measured scaling factors,

$$\frac{n_i}{n_0} = \frac{\alpha_i}{\alpha_0}.$$

If each species dominates the APS spectrum over some range of energy, the scaling factors $\alpha_i$ and thereby the densities $n_i$ can be determined quite accurately.

APS spectra measured at $m/e = 28$ are shown in Fig. 5(a). Five separate curves are plotted, scaled to an common ordinate at 45 eV. One spectrum was recorded with the discharge off and the remaining four with the discharge on at various discharge currents. Only ground state molecules are present when the discharge is off and a well-defined ionization threshold of 15.5 eV is observed in this case. Considering the pertinent electronic configurations of Table III, the minimum energy ionization pathway for ground state molecular nitrogen is the removal of an electron from the highest orbital, namely a $3\sigma_g$ electron. The ionization energy of 15.6 eV[35] is in good agreement with the observed threshold. The APS threshold is seen to shift down by ~5 eV when the

TABLE III. Electronic configurations and energies for selected neutral and ionic molecular nitrogen states (Refs. 37 and 45).

| Molecule | State | Configuration $2\sigma_g$ | $2\sigma_u$ | $1\pi_u$ | $3\sigma_g$ | $1\pi_g$ | Energy (eV) | Dissociation energy (eV) |
|---|---|---|---|---|---|---|---|---|
| $N_2$ | $X\,^1\Sigma_g^+$ | 2 | 2 | 4 | 2 | | 0 | 9.759 |
| | $A\,^3\Sigma_u^+$ | 2 | 2 | 3 | 2 | 1 | 6.169 | 3.590 |
| | $B\,^3\Pi_g$ | 2 | 2 | 4 | 1 | 1 | 7.353 | 4.790 |
| | $W\,^3\Delta_u$ | 2 | 2 | 3 | 2 | 1 | 7.362 | 4.781 |
| | $a'\,^1\Sigma_u^-$ | 2 | 2 | 3 | 2 | 1 | 8.399 | 6.128 |
| $N_2^+$ | $X\,^2\Sigma_g^+$ | 2 | 2 | 4 | 1 | | 15.581 | 8.713 |
| | $A\,^2\Pi_u$ | 2 | 2 | 3 | 2 | | 16.699 | 7.595 |

corona discharge is on. To ascribe the shift to electronic excitation, it is necessary to eliminate other internal degrees of freedom as contributing factors, particularly vibrational excitation.[36] The measured beam velocity implies an effective source temperature of several thousand degrees, ample to populate high vibrational states. Moreover, the rapid drop in beam density of a free-jet expansion often results in too few collisions to relax this degree of freedom[29] so that vibrationally excited molecules survive into the terminal beam. Yet vibrations alone cannot account for the observed threshold shift for the following reasons. Dipole–dipole transitions among vibrational states of the molecular $X\,^1\Sigma_g^+$ ground state are forbidden, making the vibrational states metastable. Franck–Condon factors for the transition from the ground state neutral molecule, $X\,^1\Sigma_g^+$, to the ground state molecular ion, $X\,^2\Sigma_g^+$, are greatest for equal vibration number, $v' = v''$.[37] Thus a neutral-to-ion transition is most likely between equal vibrational levels. The spacing of the vibrational levels is almost identical for the neutral and ionic molecules, however, the difference being only 0.51 eV for the $v' = v'' = 20$ compared to $v' = v'' = 1$. Hence vibrational contributions upon ionization are at most ~0.5 eV, much less than the observed ~5 eV threshold shift.

To ionize triplet metastable molecular $A\,^3\Sigma_u^+$ to ground state molecular ionic $X\,^2\Sigma_g^+$, Table III indicates that a two step transition is required, namely removal of a $1\pi_g$ electron followed by excitation of a $3\sigma_g$ electron into the $1\pi_u$ orbital. A two-step event is unlikely for the 2064 m/s beam molecule, which spends only ~7 $\mu$s in the 14 mm long detector ionization region. More likely is a single-step process of removing just the outmost $1\pi_g$ electron. The resulting molecular ion is then not in its ground state but rather in the excited $A\,^2\Pi_u$ state, 16.70 eV above the ground state of neutral molecular nitrogen. The ionization threshold for this transition is $(16.70 - 6.17) = 10.53$ eV, in good agreement with the measured threshold of Fig. 5(a).

The metastable content of the nondissociative ($m/e = 28$) signal is extracted by fitting the APS spectra as illustrated in Fig. 6(a). Published cross sections[38] for nondissociative electron impact ionization of ground state $X\,^1\Sigma_g^+$ (open circles) and metastable $A\,^3\Sigma_u^+$ (open triangles) are summed and superimposed (solid line curves) with the constituent cross section curves scaled in ordinate to optimize the fit of their sum to the measured data (closed squares).

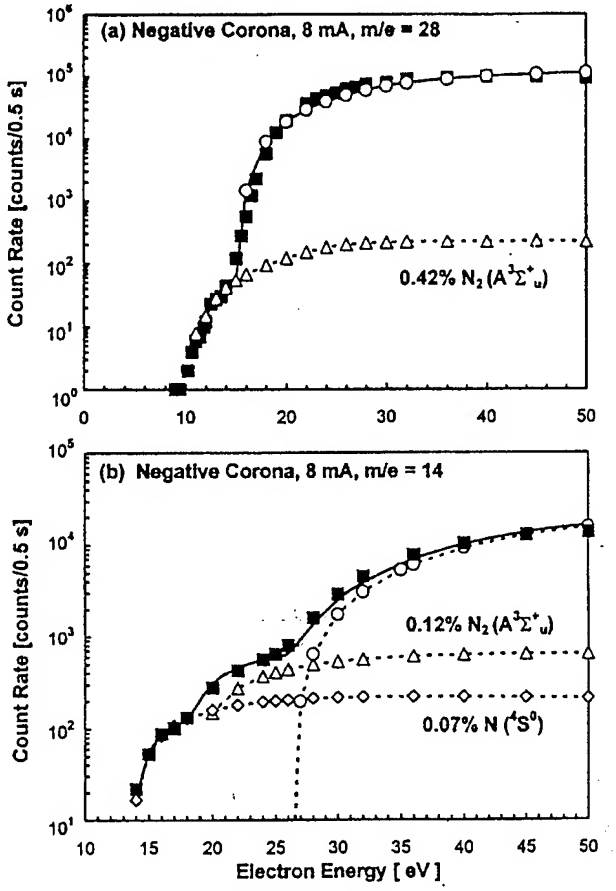


FIG. 6. Decomposition of APS curves into contributions from various activation states of nitrogen for a negative corona CDSFJ at 8 mA discharge current. Data are shown for the (a) $m/e=28$ and (b) $m/e=14$ ionization channels. The data (closed squares) have been fitted (solid curve) by scaling and summing cross sections for ground state $X\,^1\Sigma_g^+$ nitrogen molecules (circles), metastable $A\,^3\Sigma_u^+$ molecules (triangles), and $^4S^0$ nitrogen atoms (diamonds). The scaling factors yield the relative concentrations, specified in the plot as a mole fraction of the total beam.

The absence of ground state ionization below the 15.6 eV threshold and the negligible contribution of metastable ionization above ~20 eV allow the individual scaling factors and thereby the relative fractions of these two species to be determined quite precisely. An excellent fit to these $m/e=28$ data is produced by summing only the metastable $A\,^3\Sigma_u^+$ and ground state $X\,^1\Sigma_g^+$ cross sections, indicating that metastable molecular $W\,^3\Delta_u$ is present only in minute quantities, if at all. From the fitting factors of Fig. 6 (a) and incorporating the 4.3% fragmentation factor, the $A\,^3\Sigma_u^+$ signal appearing on $m/e=28$ comprises a 0.42% mole fraction of the total beam.

TABLE IV. Electronic configurations for selected states of atomic nitrogen (Ref. 56).

| Symbol | Configuration | Ionization potential (eV) |
|---|---|---|
| $N\,^4S^0$ | $2s^22p^3$ | 14.549 |
| $N\,^2D^0$ | $2s^22p^3$ | 12.169 |
| $N\,^2P^0$ | $2s^22p^3$ | 10.969 |

TABLE V. Relevant appearance potential thresholds, both dissociative and nondissociative, for ground state and long-lived excited states of molecular nitrogen as computed from the state energies of Table III.

| Initial $N_2$ state | Final $N_2^+$ state | Nondissociative threshold (eV) | Dissociative threshold (eV) |
|---|---|---|---|
| $N_2(X\,^1\Sigma_g^+)$ | $N_2^+(X\,^2\Sigma_g^+)$ | 15.581 | 24.294 |
| $N_2(A\,^3\Sigma_u^+)$ | $N_2^+(A\,^2\Pi_u)$ | 10.530 | 18.125 |
| $N_2(a'\,^1\Sigma_u^-)$ | $N_2^+(A\,^2\Pi_u)$ | 8.303 | 15.898 |
| $N_2(W\,^3\Delta_u)$ | $N_2^+(A\,^2\Pi_u)$ | 9.337 | 16.932 |

A similar process is followed for the $m/e=14$ APS spectrum of the negative corona, as shown in Fig. 5 (b). Dissociative ionization of $A\,^3\Sigma_u^+$ is a two-step process, with ionization to form molecular $N_2^+$ followed by dissociation into N and $N^+$ (Ref. 39) and detection of the $N^+$ ion. This contribution to the $m/e=14$ signal must be separated from that of atomic nitrogen. Ground state atomic nitrogen is often present in discharges[40] where it is known to quench the $A\,^3\Sigma_u^+$ state.[41,42] Relevant electronic configurations of atomic

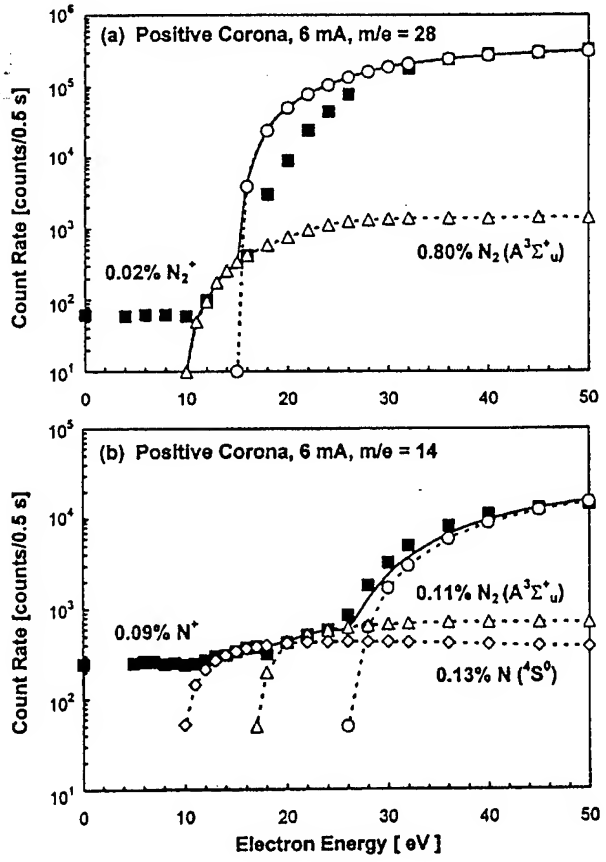


FIG. 7. APS decomposition as in Fig. 6 for (a) $m/e=28$ and (b) $m/e=14$ but here for a positive corona CDSFJ of 100% nitrogen at a discharge current of 6 mA. The constant background count rate at low electron impact energy reveals a small but nonzero presence of ions in the terminal beam.

-31- (Author to edited question: Fig 6. is correct)

TABLE VI. Concentration of active nitrogen species in a-CDSFJ beam of pure nitrogen, expressed as a number fraction of the total beam. The fractions are extracted from fits to appearance potential spectra, measured at mass-to-charge ratios of $m/e=28$ and 14. APS spectra for the 8 and 6 mA discharges are shown in Figs. 6 and 7, respectively.

| | | $m/e=14$ | | $m/e=28$ | |
|---|---|---|---|---|---|
| Corona polarity | Discharge current (mA) | $N\ ^4S^0$ (%) | $N_2\ A\ ^3\Sigma_u^+$ (%) | $N_2\ A\ ^3\Sigma_u^+$ (%) | Total activated (%) |
| Neg. | 18 | 0.18 | 0.26 | 1.30 | 1.74 |
| Neg. | 8 | 0.07 | 0.12 | 0.42 | 0.61 |
| Pos. | 6 | 0.13 | 0.11 | 0.80 | 1.04 |

nitrogen are listed in Table IV. The measured ionization threshold of ~14 eV fits none of the dissociative thresholds of Table V and must therefore be due to atomic nitrogen. Excited atomic states, such as $^2P^0$ or $^2D^0$, can be excluded on the basis of their low ionization energies. With a 14.5 eV ionization energy, ground state $^4S^0$ is the obvious candidate. The APS spectrum at $m/e=14$ was therefore fitted with three curves representing (1) dissociative ionization of ground state molecular $X\ ^1\Sigma_g^+$, (2) dissociative ionization of metastable molecular $A\ ^3\Sigma_u^+$, and (3) ionization of ground state atomic $^4S^0$. Cross sections for electron impact dissociative ionization of $X\ ^1\Sigma_g^+$ are known.[43–45] Those for $^4S^0$ have been measured[46] and tabulated[47] but are unsuitable for accurate fitting due to substantial error bars near threshold. No cross sections are available for dissociative ionization of $A\ ^3\Sigma_u^+$ state.[48] To represent these latter two curves, functional forms as suggested by Krishnakumar *et al.*[49] were fitted to the APS data in the range of low impact energy. The curves, which approach asymptotic limiting values above 45 eV, were summed to that for ground state molecular ionization and scaled to fit the APS data at high energy. The relative fractions of the three species were then taken from the values of the curves at 45 eV. As shown in Fig. 6 (b) for an 8 mA negative corona discharge, the fit can be excellent, reproducing even shoulders in the data at the onset of $A\ ^3\Sigma_u^+$ ionization (18.1 eV) and $X\ ^1\Sigma_g^+$ ionization (24.3 eV). This instills confidence in the use of the generic functional forms and in the resulting scaling factors. Incorporating the 4.3% fragmentation ratio, the metastable $A\ ^3\Sigma_u^+$ and atomic $^4S^0$ contributions to the $m/e=14$ peak are found to comprise 0.12% and 0.07% mole fraction of the total beam, respectively.

Appearance potential spectra were also recorded for positive corona discharges, as illustrated in Fig. 7. By fitting the APS curves for $m/e=28$ and $m/e=14$ in the same manner as for the negative corona, the relative fractions of atomic and metastable species in the positive CDSFJ were extracted. One striking difference is the presence of a constant background signal in both the $m/e=28$ and $m/e=14$ APS spectra of the positive corona. This extended down to zero electron impact energy and persisted even with the detector ionizer off, revealing $N^+$ and $N_2^+$ ions in the terminal beam. From the measured background signals of Fig. 7, these ions are calculated to comprise 0.09% and 0.02%, respectively, of the positive CDSFJ terminal beam.

The information extracted from Figs. 6 and 7 is summarized in Table VI. Also included are results for an 18 mA negative corona, which represents the current "best case" for absolute $A\ ^3\Sigma_u^+$ production (1.56%). The $A\ ^3\Sigma_u^+$ metastable state is by far the dominant activated species in all instances. Atomic nitrogen is present at typically 10% or less of the $A\ ^3\Sigma_u^+$ concentration. The presence of $N^+$ and $N_2^+$ ions and a somewhat lower $A\ ^3\Sigma_u^+$ content make the positive CDSFJ of lesser interest for state selective $A\ ^3\Sigma_u^+$ growth. Ions can easily be removed from the terminal beam by electrostatic or electromagnetic deflection, however, and the different ratio of atoms to metastable molecules in the various coronas might allow the relative growth characteristics of the atoms and metastables to be investigated.

For growth experiments it is the flux of excited molecular species at the growth surface that is of interest. With knowledge of excited state beam fractions and with absolute pitot measurements of the terminal beam intensity, the appropriate excited state fluxes at any desired working distance from the source are easily computed. The total activated nitrogen fluxes are complied in Table VII for a 64 cm source-to-target distance. Fluxes of a few tenth of one monolayer per second are readily achieved, corresponding to a growth rate of one to several hundred angstrom per hour. This is

TABLE VII. Total CDSFJ flux of activated nitrogen (molecular plus atomic) as extracted from appearance potential spectroscopy and pitot measurements. Roughly 90% of the total activated nitrogen is $A\ ^3\Sigma_u^+$. For the 100% $N_2$ 18 mA beam, the overall best values are listed (first row) along with averages over 27 actual III–N nitride growth runs totaling 110 h (second row).

| Gas | Polarity | Total beam intensity ($10^{18}$ No./sr/s) | Discharge current (mA) | Activated species fraction (%) | Activated species flux ($10^{13}$ No./cm$^2$/s) |
|---|---|---|---|---|---|
| 100% $N_2$ | Neg. | 6.47 | 18 (best) | 1.74 | 2.75 |
| | Neg. | 4.30 | 18 (avg) | 1.68 | 1.67 |
| | Neg. | 6.66 | 14 | 0.88 | 1.43 |
| | Neg. | 6.04 | 11 | 0.80 | 1.18 |
| | Neg. | 5.75 | 8 | 0.61 | 0.85 |
| | Pos. | 1.84 | 6 | 1.04 | 0.47 |
| 20% $N_2$/Ar | Neg. | 1.20 | 18 | 4.96 | 1.45 |
| 60% $N_2$/Ar | Neg. | 1.48 | 18 | 2.71 | 0.98 |

meager for commercial use but more than ample for research into GaN growth via $A\,^3\Sigma_u^+$ molecules. As apparent in Fig. 5, the beam fraction and therefore the flux of excited species increases significantly with increased discharge current. Optimum fluxes were obtained when the graphite skimmer had a sharp, pristine leading edge. Yet the averaged flux maintained over 100 h of operation and skimmer blunting was not even a factor of 2 less than this optimum.

Nitrogen/argon mixtures also yielded the $A\,^3\Sigma_u^+$ state. Measurements were made at mole fractions ranging from pure nitrogen down to 10% nitrogen, below which insufficient intensity was present for accurate APS spectra. The metastable flux was highest at 20% and declined at both higher and lower concentrations. A negative CDSFJ of 20% nitrogen in argon provided essentially the same flux of excited species as with 100% nitrogen gas. Since the nitrogen velocity in this dilute "seeded" beam is lower by roughly $(m_{Ar}/m_{N_2})^{1/2}$,[29] it follows that the absolute density of excited states must be even higher in the mixture than in the pure nitrogen beam.

## IV. CONCLUSION AND RECOMMENDATIONS

The corona discharge supersonic free-jet beam supplies $A\,^3\Sigma_u^+$ metastable nitrogen molecules at a typical intensity of $6\times10^{16}$ metastables $sr^{-1}\,s^{-1}$, which is two orders of magnitude higher than intensities reported for rare gas metastables.[15,17] This provides an $A\,^3\Sigma_u^+$ flux of $1.5\times10^{13}$ metastables $cm^{-1}\,s^{-1}$ at a distance of 64 cm from the nozzle, sufficient to experimentally test III–N growth via $A\,^3\Sigma_u^+$.[13,14] Commercial $A\,^3\Sigma_u^+$ growth would require higher fluxes by at least one order of magnitude. Similarity laws for glow discharges[50] suggest that gains might be realized by simply decreasing the diameter of the CDSFJ nozzle and operating at higher nozzle stagnation pressure. Terminating the corona discharge on the skimmer,[17] rather than on a reference electrode near the nozzle, might also be beneficial. Reducing the source-to-substrate distance to 20 cm would produce a tenfold flux gain. To maintain beam uniformity, an array of miniature CDSFJ nozzles would then be of interest. Quartz capillary tubing is easily "pulled" to rupture at a neck diameter of under 1 $\mu$m (Ref. 51) and miniature nozzle tubes fabricated in this fashion could be bundled to form a nozzle array.

## ACKNOWLEDGMENT

This research was supported in part by Grant No. N00014-96-1-0962 of the Office of Naval Research.

[1] S. Nakamura and G. Fasol, *The Blue Laser Diode* (Springer, Berlin, 1997).
[2] J. W. Orton and C. T. Foxton, Rep. Prog. Phys. **61**, 1 (1998) and references therein.
[3] W. Goddard III, 45th International Symposium of the AVS, Baltimore, MD, 1998. (unpublished)
[4] A. Sellidj, B. A. Ferguson, T. J. Mattord, B. G. Streetman, and C. B. Mullins, Appl. Phys. Lett. **68**, 3314 (1996).
[5] S. E. Hooper, C. T. Foxton, T. S. Cheng, L. C. Jenkins, D. E. Lacklison, J. W. Orton, T. Bestwick, A. Kean, M. Dawson, and G. Duggan, J. Cryst. Growth **155**, 157 (1995).
[6] R. W. McCullough, J. Geddes, J. A. Croucher, J. M. Woolsey, D. P. Higgins, M. Schlapp, and H. B. Gilbody, J. Vac. Sci. Technol. A **14**, 152 (1996).
[7] R. P. Vaudo, J. W. Cook, Jr., and J. F. Schetzina, J. Vac. Sci. Technol. B **12**, 1232 (1994).
[8] W. C. Hughes, W. H. Rowland, Jr., M. A. L. Johnson, S. Fujita, J. W. Cook, Jr., J. F. Schetzina, J. Ren, and J. A. Edmond, J. Vac. Sci. Technol. B **13**, 1571 (1995).
[9] T. D. Moustakas, Mater. Res. Soc. Symp. Proc. **395**, 111 (1995).
[10] A. Anders, N. Newman, M. Rubin, M. Dickinson, E. Jones, P. Phatak, and J. Gassmann, Rev. Sci. Instrum. **67**, 905 (1996).
[11] M. A. Cappelli, A. E. Kull, K. Schwender, H. Lee, S. J. Harris, Jr., and J. Mroczkowski, Mater. Lett. **31**, 161 (1997).
[12] F. J. Grunthaner, R. Bicknell-Tassius, P. Deelman, P. J. Grunthaner, C. Bryson, E. Snyder, J. L. Giuliani, J. P. Apruzese, and P. Kepple, J. Vac. Sci. Technol. A **16**, 1615 (1998).
[13] D. C. Jordon, Ph.D. thesis, Arizona State University, 1999.
[14] D. C. Jordan, I. S. T. Tsong, D. J. Smith, and R. B. Doak, Appl. Phys. Lett. ■■, ■■■■ (2000). 77, 3030
[15] *Atomic and Molecular Beam Methods, Vols. I & II*, edited by G. Scoles (Oxford University, Oxford, 1988).
[16] P. C. Engelking, Rev. Sci. Instrum. **57**, 2274 (1986).
[17] D. Neuerschäfer, Ch. Ottinger, and A. Sharma, Chem. Phys. **117**, 133 (1987).
[18] J. Q. Searcy, Rev. Sci. Instrum. **45**, 589 (1974).
[19] E. L. Leasure, C. R. Mueller, and T. Y. Ridley, Rev. Sci. Instrum. **46**, 635 (1975).
[20] D. W. Fahey, L. D. Schearer, and W. F. Parks, Rev. Sci. Instrum. **49**, 503 (1978).
[21] D. W. Fahey, W. F. Parks, and L. D. Schearer, J. Phys. E **13**, 381 (1980).
[22] A. T. Droge and P. C. Engelking, Chem. Phys. Lett. **96**, 316 (1983).
[23] P. C. Engelking, Chem. Rev. **91**, 339 (1991).
[24] K. R. Comer and S. C. Foster, Chem. Phys. Lett. **202**, 216 (1993).
[25] K. P. Huber and M. Vervloet, J. Mol. Spectrosc. **153**, 17 (1992).
[26] I. Hadj Bachir, T. R. Huet, J. L. Destombes, and M. Vervloet, Chem. Phys. Lett. **270**, 533 (1997).
[27] D. J. Auerbach, *Atomic and Molecular Beam Methods, Vol. I & II*, edited by G. Scoles (Oxford University, Oxford, 1988), Chap. 14 in Vol. 1.
[28] D. C. Jordan, R. Barling, and R. B. Doak, Rev. Sci. Instrum. **70**, 1640 (1999).
[29] D. R. Miller, *Atomic and Molecular Beam Methods, Vol. I & II*, edited by G. Scoles (Oxford University, Oxford, 1988), Chap. 2 in Vol. 1.
[30] For color images, see V. M. Torres, D. C. Jordan, I. S. T. Tsong, and R. B. Doak, in *Atomic and Molecular Beams, Part* edited by R. Campargue (Springer-Verlag, Berlin, 2000). VII Chap. 8
[31] L. B. Loeb, *Electrical Coronas* (University of California, Berkley, 1965).
[32] I. Gallimberti, J. Phys. D **5**, 2179 (1972).
[33] E. Marode, J. Appl. Phys. **46**, 2005 (1975).
[34] K. Kondo and N. Ikuta, J. Phys. D **13**, L33 (1980).
[35] H. S. W. Massey, E. H. S. Burhop, and H. B. Gilbody, *Electronic and Ionic Impact Phenomena, Vol. II* (Clarendon, Oxford, 1969), p. 956.
[36] S. N. Foner and R. L. Hudson, J. Chem. Phys. **37**, 1662 (1962).
[37] A. Lofthus and P. H. Krupenie, J. Phys. Chem. Ref. Data **6**, 113 (1977).
[38] P. B. Armentrout, S. M. Tarr, A. Dori, and R. S. Freund, J. Chem. Phys. **75**, 2786 (1981).
[39] P. C. Cosby, J. Chem. Phys. **98**, 9544 (1993).
[40] G. Cernogora, L. Hochardt, M. Touzeau, and C. M. Ferreira, J. Phys. B **14**, 2977 (1981).
[41] K. L. Wray, J. Chem. Phys. **44**, 623 (1966).
[42] J. A. Meyer, D. W. Setser, and D. H. Stedman, J. Phys. Chem. **74**, 2238 (1970).
[43] A. Crowe and J. W. McConkey, J. Phys. B **6**, 2108 (1973).
[44] B. Van Zyl and T. M. Stephen, Phys. Rev. A **50**, 3164 (1994).
[45] Y. Itikawa, M. Hayashi, A. Ichimura, K. Onda, K. Sakimoto, K. Takayanagi, M. Nakamura, H. Nishimura, and T. Takayanagi, J. Phys. Chem. Ref. Data **15**, 985 (1986).
[46] D. Rapp, P. Englander-Golden, and D. D. Briglia, J. Chem. Phys. **42**, 4081 (1965).
[47] E. Brook, M. F. A. Harrison, and A. C. H. Smith, J. Phys. B **11**, 3115 (1978).
[48] P. B. Armentrout and K. H. Becker (private communication).
[49] E. Krishnakumar and S. K. Srivastava, J. Phys. B **21**, 1055 (1988).
[50] *Handbuch der Physik, Vol. XXII*, edited by S. Flügge (Springer-Verlag, Berlin, 1956), p. 70.

[51] J. Braun, P. K. Day, J. P. Toennies, G. Witte, and E. Neher, Rev. Sci. Instrum. 68, 3001 (1997).
[52] D. C. Cartwright, S. Trajmar, A. Chutjian, and W. Wiliams, Phys. Rev. A 16, 1041 (1977).
[53] D. E. Shemansky and N. Carleton, J. Chem. Phys. 51, 682 (1969); D. E. Shemansky, *ibid.* 51, 689 (1969).
[54] H.-J. Werner, J. Kalcher, and E.-A. Reinsch, J. Chem. Phys. 81, 2420 (1984) and references tabulated therein.
[55] W. Benesch, Phys. Rev. A 19, 445 (1979).
[56] R. F. Bacher and S. Goudsmit, *Atomic Energy States* (Greenwood, New York, 1968), pp. 301–306.
[57] R. W. B. Pearse and A. G. Gaydon, *The Identification of Molecular Spectra* (Wiley, New York, 1963).

## V. $A^3\Sigma_U^+$ INCORPORATION EFFICIENCY

Using the corona discharge supersonic free-jet (CD-SFJ), several dozen III-N thin films were grown and analyzed. The films were characterized ex situ by Rutherford backscattering spectrometry (RBS), scanning electron microscopy (SEM), electron channeling pattern (ECP), atomic force microcopy (AFM), and transmission electron microscopy (TEM). Both hexagonal and cubic GaN films could be grown with an abrupt, well ordered epitaxial interface on 6H-SiC(0001) and with good crystallinity in the film. Good epitaxial interfaces were obtained even when GaN was grown directly on SiC. The measured incorporation efficiency (N atoms attaching per incident $N^2$ molecule) approached 100% and was independent of the substrate temperature from 600 to 900°C. Measurements of incorporation efficiency as a function of beam energy indicated that direct dissociative molecular chemisorption was underlying growth mechanism. These measurements were described in the following paper, "III-N Semiconductor Growth with Activated Nitrogen: A State-Specific Study of $A^3\Sigma_u^+$ Metastable $N_2$ Molecules," D.C. Jordan, I.S.T. Tsong, D.J. Smith, and R.B. Doak, Appl. Phys. Lett, 77, 3030-3032 (2000).

# III-N semiconductor growth with activated nitrogen: State-specific study of $A^3\Sigma_u^+$ metastable $N_2$ molecules

D. C. Jordan,[a] I. S. T. Tsong,[a] David J. Smith,[a),b)] B. J. Wilkens,[b)] and R. B. Doak[a),c)]
*Arizona State University, Tempe, Arizona 85287*

(Received 22 May 2000; accepted for publication 15 September 2000 )

High quality epitaxial III-N semiconductor films, ranging in thickness from 300 to 900 Å, have been grown using $A^3\Sigma_u^+$ metastable nitrogen molecules. The work employed a corona discharge supersonic free-jet to generate a molecular beam containing exclusively the $A^3\Sigma_u^+$ activation state in an otherwise ground state $N_2$ beam. AlN films were grown on 6H–SiC(0001) and Si(001) substrates. GaN films were grown on the same substrates and on buffer layers of AlN deposited *in situ* on 6H–SiC(0001). The N-atom incorporation efficiency (the number of N atoms attaching to a III–N surface per incident $A^3\Sigma_u^+$ molecule) approached 100% and was independent of substrate temperature from 600 to 900 °C, implying direct molecular chemisorption of the $A^3\Sigma_u^+$. These measurements support theoretical predictions that $A^3\Sigma_u^+$ is an ideal precursor for III–N growth.
 [S0003-6951(00)02645-0]

In recent years there has been rapid progress in III–N semiconductor technology.[1,2] Metalorganic vapor-phase epitaxy (MOVPE) has emerged as the leading III–N growth process, generally utilizing ammonia and trimethylmetallics as the precursors for nitrogen and group III metals, respectively. Blue/green/amber light-emitting diodes (LEDs) are now commercially fabricated via MOVPE,[3,4] as are blue/violet heterostructure laser diodes (LDs).[5] In contrast, and despite potential advantages over MOVPE, progress in molecular beam epitaxy (MBE) of III–N semiconductors has been slow. MBE provides a pristine ultrahigh vacuum (UHV) growth environment, a precise control over layer-by-layer composition, and the ability to monitor growth *in situ* via standard surface science tools. MBE also offers a wide choice of sources, including effusive or supersonic beams of MOVPE species, electrical discharge free jets of activated nitrogen, and effusive beams of high purity metals. To date, however, MBE has generally delivered inferior III–N material to MOVPE. In one comparison, MOVPE fabrication yielded significantly less dislocation-induced shorting in blue/violet LEDs than did plasma-source MBE.[6] Similarly, epitaxial lateral overgrowth (ELO) with MOVPE yielded single crystal GaN overlayers whereas plasma-source MBE resulted in polycrystalline growth.[7] On the other hand, Ploog and co-workers[8] report that, with improved substrate preparation and careful *in situ* monitoring, MBE can indeed yield high quality films. Improved understanding and further optimization of MBE III–N growth processes clearly remain important goals.

Of interest in this regard are MBE discharge sources. To conduct MBE with gaseous molecular nitrogen the strong $N_2$ triple bond must be weakened or broken by electrical excitation in a microwave [electron cyclotron resonance (ECR)], radio frequency (rf),[2] or other such electrical discharge.[9] These discharges invariably produce a broad spectrum of activated species, including electronically excited molecules and atoms and possibly even molecular and/or atomic ions. In a comparative study of specific ECR and rf discharge sources, Hughes *et al.*[10] attempted to correlate GaN film quality with the optical emission of the discharge cavity, considering specifically molecular emission in the first and second positive series (denoted "1+" and "2+," respectively) and on atomic and ionic lines. The ECR source displayed less atomic emission and more 2 + molecular emission than the rf source. It also produced ionic $N_2^+$ emission whereas the rf discharge did not. Superior quality film growth resulted with the rf discharge source. While acknowledging known detrimental effects of energetic ions,[11] Hughes *et al.* nonetheless concluded that optimum growth correlated to the presence of 1+ molecular emission and atomic emission,[10] indicating that a combination of $A^3\Sigma_u^+$ nitrogen and atomic nitrogen is desired. Newman drew similar conclusions for the hollow-anode discharge.[12] Optical emission of a discharge cavity, however, may be a poor indicator of the activated species actually present at the growth surface, particularly if nonemitting species such as $A^3\Sigma_u^+$ are involved. Much preferred would be a beam containing only a single activation state. Corona discharge supersonic free-jets (CD-SFJ) offer this capability for $A^3\Sigma_u^+$ $N_2$ molecules.

The reaction of activated nitrogen with Ga- and N-terminated GaN films has been investigated theoretically by Goddard and Muller.[12,13] While many activation states of nitrogen deliver sufficient free energy to surmount activation barriers,[12] Goddard and Muller concluded that $A^3\Sigma_u^+$ is the preferred species for GaN growth by virtue of its lower reaction exothermicity and because it is a molecule.[13] Of the energy released when the molecular $A^3\Sigma_u^+$ reacts, it is predicted that most is carried away as kinetic energy by one of the two atoms, leading to efficient attachment of the second atom in a nearly quiescent state.[14] In contrast, the reaction of atomic nitrogen is strongly exothermic (3.87 eV) with no means of dissipating energy other than through phonon creation or sputtering. This is predicted to yield poor N incorporation and possibly even sputtering or etching.[13]

[a)]Present address: Department of Physics and Astronomy.
[b)]Present address: Center for Solid State Science.
[c)]Electronic mail: bdoak@asu.edu

 

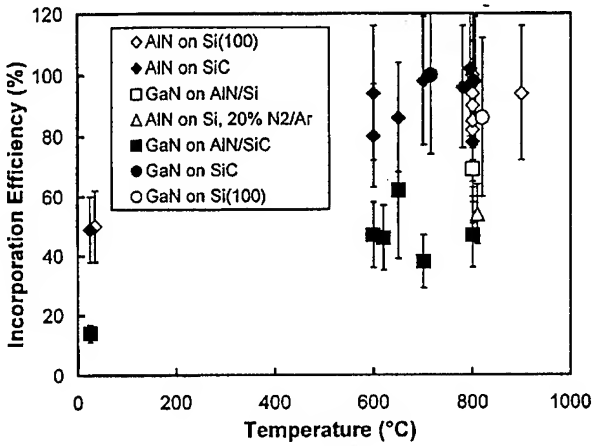


FIG. 1. $A^3\Sigma_u^+$ incorporation efficiency, defined as the number of N atoms attaching to the III–N film per $A^3\Sigma_u^+$ molecule incident onto the surface, measured as a function of substrate deposition temperature.

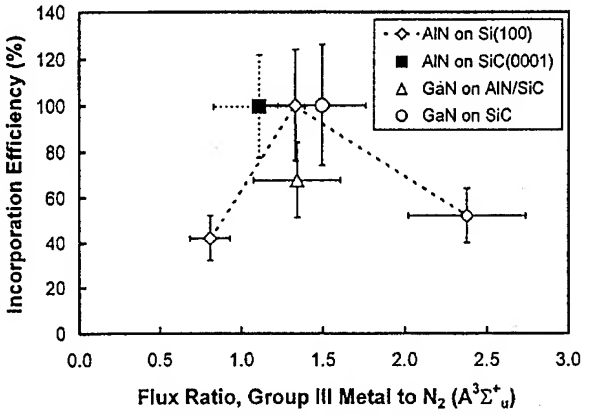


FIG. 2. Incorporation efficiency measured as a function of the ratio of the group III metal flux to the $N_2$ $A^3\Sigma_u^+$ flux.

The presence of $A^3\Sigma_u^+$ in both rf and ECR discharges is evidenced by 1+ and 2+ emission from both sources,[10] revealing the relaxation cascade through the manifold of excited $N_2$ triplet states to populate the $A^3\Sigma_u^+$ state. Since the $A^3\Sigma_u^+$ state does not deexcite on the scale of MBE transit times, it can be employed much in the fashion of any stable MBE reactant. Even though it is possible to optimize the $A^3\Sigma_u^+$ yield in a conventional plasma discharge by adjusting the gas flow rate and discharge power, a corona discharge supersonic free-jet offers a far more effective means of exclusively generating this species. In a CD-SFJ, a corona discharge is struck in the high pressure region just within the supersonic nozzle of a freejet expansion. As the gas flow expands through the nozzle throat and into vacuum, the rapid decrease in flow density terminates the discharge. Spontaneous relaxation and expansion cooling then return all short-lived excited states to the ground state, leaving $A^3\Sigma_u^+$ as the dominant excited species in the terminal molecular beam. Nearly 2% mole fraction of a terminal CD-SFJ nitrogen beam can be $A^3\Sigma_u^+$,[15] the remaining beam consisting of groundstate $N_2(X^1\Sigma_g^+)$[16] plus a negligible ($<0.1\%$) fraction of ground-state N atoms ($^4S^0$). Thus the CD-SFJ source allows growth via $A^3\Sigma_u^+$ alone, in the absence of all other activation states.

Using the CD-SFJ, III–N film growth was carried out for a total beam intensity, fractional percentage of $A^3\Sigma_u^+$ species, and resulting $A^3\Sigma_u^+$ flux which averaged $4.3\times10^{18}$ $N_2$/sr/s, 1.68%, and $1.7\times10^{13}$ metastables/cm$^2$/s, respectively, over the course of the depositions. This yielded GaN growth at the rate of one to several hundred angstrom per hour, marginal for commercial processing but more than adequate for investigating the reaction chemistry of the $A^3\Sigma_u^+$ state. Films of AlN and GaN were grown to thickness of 300–900 Å on Si(100) and on Si-terminated 6H–SiC(0001). GaN films were also grown on AlN buffer layers deposited *in situ* on SiC. The resulting films were investigated *ex situ* by Rutherford backscattering spectrometry (RBS), scanning electron microscopy (SEM), electron channeling patterns (ECP), atomic force microscopy (AFM), and transmission electron microscopy (TEM). RUMP simulations of the RBS spectra[17] provided areal densities of the resulting III–V nitride films. Combined with absolute measurements of the incident flux of $A^3\Sigma_u^+$, this allowed the nitrogen incorporation efficiency (defined to be the number of N atoms attaching per $A^3\Sigma_u^+$ molecule incident) to be computed.

A tabulation of this incorporation efficiency is plotted in Fig. 1 as a function of the substrate deposition temperature. Efficiencies of 100% are approached for GaN or AlN grown directly on Si or SiC, verifying that $A^3\Sigma_u^+$ is a highly reactive and easily incorporated species for III–N MBE growth and strongly supporting the theoretical modeling of Goddard and Muller.[13] The efficiencies for GaN deposited on AlN/SiC are somewhat lower, ~50%, and this is tentatively ascribed to the rougher surface morphology and decreased adatom mobility in that case. The incorporation efficiency was found to be independent of the substrate temperature from 600 to 900 °C, indicating that direct dissociative chemisorption is the underlying process for $A^3\Sigma_u^+$ attachment. Both the incorporation efficiency and the growth rates dropped dramatically below 600 °C, a known consequence of the reduced mobility of group III metal atoms on the surface at these lower temperatures.[18]

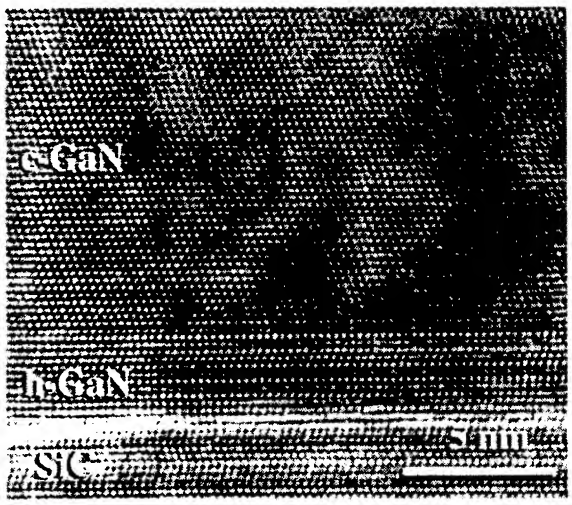


FIG. 3. Cross-sectional transmission electron micrograph showing cubic phase GaN grown on 6H–SiC(0001) at 700 °C. Abrupt, well ordered epitaxial interfaces were obtained. This particular film grew as hexagonal GaN for the first 10–12 layers.

For AlN growth on Si(001), the incorporation efficiency decreased from 90% to 50% when a 20% $N_2$/Ar mixture was used instead of pure $N_2$. "Seeding" nitrogen into a heavier inert carrier gas in this fashion reduces the kinetic energy of the nitrogen molecules,[19] from 0.65 eV for 100% $N_2$ to 0.35 eV for the 20% $N_2$/Ar mixture. Optical emission spectra showed the terminal excited state distribution in the mixture to be essentially identical to that of the pure beam. Since the inert, low energy, neutral argon has no influence on reaction kinetics, the difference in incorporation must be attributed to the change in $N_2$ incident kinetic energy, suggesting a reaction barrier in the range of 0.5 eV for $A^3\Sigma_u^+$ growth of AlN on Si(001) substrates.

The measured incorporation efficiency is plotted in Fig. 2 as a function of the $A^3\Sigma_u^+$ flux for various growth systems. For both AlN and GaN, the incorporation efficiency peaks at a metal-to-$A^3\Sigma_u^+$ flux ratio of between 1.0 and 1.5. This agrees with the observation by many groups that metal-rich conditions yield optimum MBE growth.[2,20,21] Metal fluxes higher than this optimum value result in metal island formation and blockage of surface sites, decreasing the incorporation efficiency. Lower metal fluxes lead to an increased steady-state N-adatom coverage on the surface, increasing the recombination of N adatoms to form gaseous $N_2$ [exothermic by 2.07 eV (Ref. 13)] and thereby reducing the overall nitrogen incorporation efficiency.

Epitaxial order of the CD-SFJ deposited films was investigated by RBS, ECP, and TEM, as discussed elsewhere.[22] One typical high resolution TEM image is presented in Fig. 3. This 310 Å thick GaN film was grown at 700 °C on Si-terminated 6H–SiC(0001) without a buffer layer.[23] The abrupt, well-defined GaN/SiC interface is typical of the III–N films grown, showing that growth with $A^3\Sigma_u^+$ metastable molecules is not only a highly efficient process, but one which yields good epitaxial order.

This work was supported in part by the Office of Naval Research under Grant No. N00014-96-1-0962. Use of facilities in the ASU Center for High Resolution Electron Microscopy is acknowledged.

[1] S. Nakamura and G. Fasol, *The Blue Laser Diode* (Springer, Berlin, 1997).
[2] J. W. Orton and C. T. Foxton, Rep. Prog. Phys. **61**, 1 (1998), and references therein.
[3] S. Nakamura, M. Senoh, N. Isawa, S. Nagahama, T. Yamada, and T. Mukai, Jpn. J. Appl. Phys., Part 2 **34**, L1332 (1995).
[4] T. Mukai, H. Narimatsu, and S. Nakamura, Jpn. J. Appl. Phys., Part 2 **37**, L479 (1998).
[5] S. Nakamura, M. Senoh, A. Nagahama, N. Iwasa, T. Matsushita, and T. Mukai, Appl. Phys. Lett. **76**, 22 (2000), and references therein.
[6] M. A. L Johnson, Z. Yu, J. D. Brown, F. A. Koeck, N. A. El-Masry, H. S. Kong, J. A. Edmond, J. W. Cook, and J. F. Schetzina, MRS Internet J. Nitride Semicond. Res. **41**, 10 (1999).
[7] Z. Yu, M. A. L. Johnson, J. D. Brown, N. A. El-Masry, J. F. Muth, J. W. Cook, J. F. Schetzina, K. W. Haberern, H. S. Kong, and J. A. Edmond, MRS Internet J. Nitride Semicond. Res. **41**, 4.3 (1999).
[8] O. Brandt, R. Muralidharan, P. Waltreit, A. Thamm, A. Trampert, H. von Kierdowski, and K. H. Ploog, Appl. Phys. Lett. **75**, 4019 (1999).
[9] A. Anders, N. Newman, M. Rubin, M. Dickinson, E. Jones, P. Phatak, and A. Gassmann, Rev. Sci. Instrum. **67**, 905 (1996).
[10] W. C. Hughes, W. H. Rowland, Jr., M. A. L. Johnson, S. Fujita, J. W. Cook, Jr., and J. F. Schetzina, J. Vac. Sci. Technol. B **13**, 1571 (1995).
[11] T. C. Fu, N. Newman, E. Jones, J. S. Chan, X. Liu, M. D. Rubin, N. W. Cheung, and E. R. Weber, J. Electron. Mater. **24**, 249 (1994).
[12] N. Newman, J. Cryst. Growth **178**, 102 (1997).
[13] W. A. Goddard III, 45th International Symposium of the AVS, Baltimore, MD, 2–6 November 1998; http://www.wag.caltech.edu/home/rpm/projects/gan/gan/index.htm
[14] The calculations show a late transition state for the $N_2 A^3\Sigma_u^+$ reaction, indicating that moderate vibrational excitation of the $N_2 A^3\Sigma_u^+$ further facilitates the reaction.
[15] D. C. Jordan, C. T. Burns, and R. B. Doak, J. Appl. Phys. (to be published).
[16] The presence of ground state molecular nitrogen, $N_2 X^1\Sigma_g^+$, has no effect on the MBE growth since GaN growth from this species is possible only at tremendous overpressures [R. Madar, G. Jacob, J. Hallais, and R. Fruchart, J. Cryst. Growth **31**, 197 (1975)].
[17] L. R. Doolittle, Nucl. Instrum. Methods Phys. Res. B **9**, 344 (1985).
[18] Surface mobility of N adatoms plays no role, being negligible at these temperatures. T. Zywietz, J. Neugebauer, and M. Scheffler, Appl. Phys. Lett. **73**, 487 (1998); O. Brandt, H. Yang, and K. Ploog, Phys. Rev. B **54**, 4432 (1996).
[19] See, e.g., D. R. Miller, in *Atomic and Molecular Beam Methods*, edited by G. Scoles (Oxford University Press, Oxford, 1988), Vol. I, Chap. 2.
[20] A. R. Smith, V. Ramachandran, R. M. Feenstra, D. W. Greve, A. Ptak, T. Myers, W. Sarney, L. Salamanca-Riba, M. Shin, and M. Skowronski, MRS Internet J. Nitride Semicond. Res. **3**, 12 (1998), and references therein.
[21] A. Pavlovska, V. M. Torres, E. Bauer, R. B. Doak, I. S. T. Tsong, D. B. Thomson, and R. F. Davis, Appl. Phys. Lett. **75**, 898 (1999).
[22] D. C. Jordan, Ph.D. thesis, Arizona State University, Tempe, AZ, 1999.
[23] AFM images of this particular film (Ref. 22) revealed a morphology of incompletely coalesced islands of roughly 0.5 $\mu$m in size.

# REPORT DOCUMENTATION PAGE

*Form Approved*
*OMB No. 0704-0188*



| 1. REPORT DATE *(DD-MM-YYYY)* | 2. REPORT DATE | 3. DATES COVERED *(From - To)* |
|---|---|---|
| 15-12-00 | FINAL REPORT | 01-05096 to 30-04-99 |

**4. TITLE AND SUBTITLE**

Final Report: Construction, Characterization, And Use of an Arc-Heated Supersonic Free-Jet of Nitrogen Atoms for the Growth of GaN, AlN, and InN Thin Films

**5a. CONTRACT NUMBER**

**5b. GRANT NUMBER**
N00014-96-1-0962

**5c. PROGRAM ELEMENT NUMBER**

**6. AUTHOR(S)**
R.B. Doak

**5d. PROJECT NUMBER**
96PR06413-00

**5e. TASK NUMBER**

**5f. WORK UNIT NUMBER**

**7. PERFORMING ORGANIZATION NAME(S) AND ADDRESS(ES)**
Arizona State University
Tempe, AZ 85284

**8. PERFORMING ORGANIZATION REPORT NUMBER**

**9. SPONSORING/MONITORING AGENCY NAME(S) AND ADDRESS(ES)**
Office of Naval Research
Regional Office San Diego
4520 Executive Drive Suite 300
San Diego, CA 92121-3019

**10. SPONSOR/MONITOR'S ACRONYM(S)**
ONR

**11. SPONSORING/MONITORING AGENCY REPORT NUMBER**

**12. DISTRIBUTION AVAILABILITY STATEMENT**
Approved for Public Release

**13. SUPPLEMENTARY NOTES**

**14. ABSTRACT**

High quality epitaxial III-N semiconductor films, ranging in thickness from 300 to 900 Å, have been grown using $A^3\Sigma_u^+$ metastable nitrogen molecules. The work employed a corona discharge supersonic free-jet (CD-SFJ) to generate a molecular beam containing exclusively the $A^3\Sigma_u^+$ activation state in an otherwise ground state $N_2$ beam. AlN films were grown on 6H-SiC(0001) and Si(001) substrates. GaN films were grown on the same substrates and on buffer layers of AlN deposited *in situ* on 6H-SiC(0001). The N-atom incorporation efficiency (the number of N-atoms attaching to a III-N surface per incident $A^3\Sigma_u^+$ molecule) approached 100% and was independent of substrate temperature from 600 to 900 °C, implying direct molecular chemisorption of the $A^3\Sigma_u^+$. These measurements support theoretical predictions that $A^3\Sigma^+_u$ is an ideal precursor for III-N growth.

**15. SUBJECT TERMS**

GaN, Gallium Nitride, AlN, Aluminum Nitride, Supersonic Free-Jet, Corona Discharge, Metastable Nitrogen

| 16. SECURITY CLASSIFICATION OF: | | | 17. LIMITATION OF ABSTRACT | 18. NUMBER OF PAGES | 19a. NAME OF RESPONSIBLE PERSON |
|---|---|---|---|---|---|
| a. REPORT | b. ABSTRACT | c. THIS PAGE | | | Prof. R. Bruce DOAK |
| U | U | U | UU | 39 | 19b. TELEPONE NUMBER ( *Include area code)* 480-965-0640 |

Standard Form 298 (Rev. 8-98)
Prescribed by ANSI-Std Z39-18